PHYSICAL REVIEW D VOLUME 52, NUMBER 6 15 SEPTEMBER 1995

Neutrino oscillations in the early Universe with nonequilibrium neutrino distributions

V. Alan Kostelecký
Physics Department, Indiana University, Bloomington, Indiana 47405

Stuart Samuel*
Max-Planck-Institut für Physik, Werner-Heisenberg-Institut, Föhringer Ring 6, 80805 Munich, Germany
(Received 28 March 1995)

Around one second after the big bang, neutrino decoupling and e^+-e^- annihilation distorted the Fermi-Dirac spectrum of neutrino energies. Assuming neutrinos have masses and can mix, we compute the distortions using nonequilibrium thermodynamics and the Boltzmann equation. The flavor behavior of neutrinos is studied during and following the generation of the distortion.

PACS number(s): 95.30.Cq, 12.15.Ff, 14.60.Pq

I. INTRODUCTION

Neutrinos play a significant role both in cosmology [1] and in particle physics [2]. In cosmology, during the radiation-dominated period in the early Universe from one second after the big bang to around twenty-thousand years, neutrinos are almost as important as photons in driving the expansion of the Universe. Furthermore, nucleosynthesis and the ensuing abundances of light elements are strongly influenced by the number and nature of neutrinos. In particle physics, it is hoped that current oscillation experiments coupled with solar and atmospheric neutrino observations will lead to insight beyond the standard model. The basic idea is that interference among neutrino flavors provides a sensitive experimental probe for neutrino masses and mixings.

It is natural to ask whether neutrino oscillations affect the physics of the early Universe. Different aspects of this question have been addressed by a number of authors [3–14]. When the temperature T of the Universe is several MeV and higher, interactions keep neutrinos in thermal contact with electrons, positrons, and the primodial plasma and so oscillations cannot occur. If thermal equilibrium were maintained for all times, then the numbers of e, μ, and τ neutrinos would be equal. This would preclude flavor oscillations because, for instance, for each ν_e that converts into a ν_μ there would be a ν_μ converting into a ν_e.

However, around 1 s when T is about 1 MeV, nonequilibrium distributions develop. This effect is due to the coincidence of thermal-neutrino decoupling and e^+-e^- annihilation. As some e^+-e^- pair annihilate, they reheat photons and other electrons and positrons. The latter in turn can interact with neutrinos via the weak interactions, thereby slightly reheating the neutrinos. This reheating is both flavor and energy dependent because the neutrinos are decoupling at this time. Due to $W^\pm$ exchanges, electron neutrinos are heated somewhat more than μ and τ neutrinos. This leads to an excess of electron neutrinos over μ and τ neutrinos. Furthermore, higher-energy neutrinos interact more strongly than lower-energy neutrinos so that a relative excess of higher-energy neutrinos arises. The appearance of a flavor excess means that neutrino oscillations can occur. This potentially could affect nucleosynthesis [5].

The process generating the distorted distributions is sensitive to the timing of events in the early Universe. If the neutrinos had decoupled well before e^+-e^- annihilation, then they would have maintained Fermi-Dirac distributions. Their energies and momenta would simply have been redshifted by the inverse scale factor $R^{-1}(t)$ of the Friedmann-Robertson-Walker (FRW) cosmology. For ultrarelativistic particles, such redshifts maintain standard statistical distributions. If instead the neutrinos had decoupled well after e^+-e^- annihilation, then they would have remained in thermal equilibrium during the heating process. When they decoupled later, they would have again maintained a redshifted Fermi-Dirac distribution. In either case, no flavor asymmetry would have arisen and so no oscillations would have occurred.

The analysis of nonequilibrium neutrino distributions is not an easy undertaking, even in the absence of neutrino mixing. This problem has recently been treated in two different approaches based on the Boltzmann equation. A detailed study allowing for contributions from all tree-level scattering amplitudes, performing exactly many phase space integrations, and using numerical methods to solve the Boltzmann equation is presented in Ref. [15]. Estimates of the effects and relatively simple approximate analytical formulae for the distortion of distributions are provided in Ref. [16].

When neutrinos mix, the problem of analyzing nonequilibrium neutrino distributions becomes significantly more complicated. The complications arise not only from the simultaneous occurrence of production and oscillations but also from indirect effects modifying vacuum-oscillation behavior. These effects arise from neutrino interactions with the background gas of elec-

*Permanent address: Physics Department, City College of New York, New York, NY 10031. Electronic address: samuel@scisun.sci.ccny.cuny.edu

 ©1995 The American Physical Society

trons, positrons, and other neutrinos. In particular, neutrino-neutrino interactions can strongly affect oscillations because neutrinos in the early Universe form a dense gas and because the effects are nonlinear. These interactions enter as flavor-off-diagonal as well as flavor-diagonal terms in the effective Hamiltonian [17]. The ensuing complications can be handled using Hartree-Fock-like or density-matrix formalisms [18,19].

In previous papers [11–13], we have analyzed neutrino-flavor properties in the early Universe assuming nonequilibrium neutrino distributions based on the approximate analytical formulae of Ref. [16]. These analyses therefore disregard the role of neutrino oscillations during the generation of the nonequilibrium distributions, although various tests suggest that our qualitative results are correct.

In the current work, we obtain the equations that describe the nonequilibrium distortions of neutrino distributions when mixing is present, and we present numerical solutions of the ensuing neutrino behavior. The remainder of this introduction provides a guide to the structure of the paper.

For simplicity, we assume that mixing occurs only between two neutrinos, taken to be ν_e and ν_μ, and that the third neutrino, taken as ν_τ, does not participate in the oscillations. The analysis of nonequilibrium statistics in Ref. [15] was performed under the assumption that μ and τ neutrinos behave identically. However, with neutrino mixing, the τ neutrino cannot be disregarded because it participates in the generation of thermal distortions via e^+-e^- annihilations. The equations obtained in Ref. [15] must therefore be generalized. This is accomplished in Sec. II.

Section III reviews our formalism for dense-neutrino oscillations in the early Universe, while Sec. IV summarizes the neutrino-oscillation behavior uncovered in Refs. [11,13]. This summary is used in the discussion of our new results in Secs. VIII and IX. Section V combines the results of Secs. II and III to obtain equations that govern the production of nonequilibrium neutrino distributions in the presence of mixing.

The deviations from standard thermal distributions are generated from about 0.1 s to about 1.5 s. We call this the *production phase* because the flavor-dependent neutrino excesses are produced during this interval. By *production profile*, we mean the nonequilibrium distortions that arise at the end of the production phase. The term *pure production* is reserved for production without neutrino mixing. After about 1.5 s, neutrino decoupling is sufficiently strong that few further distortions in statistical distributions are generated. We call the period after about 1.5 s the *oscillation phase.*

One of our goals is to understand neutrino-flavor variation during the production phase. This requires computer simulations because the equations are nonlinear and relatively complicated. Issues concerning numerical methodology are discussed in Sec. VI. Some improvements are made over the work of Ref. [15] even for the pure-production case. For this reason, we have repeated the analysis of the pure-production case in Sec. VII.

Another goal is to obtain the production profile in the presence of neutrino mixing. Production profiles for various neutrino mixing angles and mass differences are presented in Sec. VIII. This section also discusses the general behavior of neutrino oscillations and related properties.

Section IX analyzes the oscillation phase. The main purpose is to check the results of Refs. [11,13]. The qualitative flavor properties described in [11,13] are confirmed. Small numerical differences are uncovered, however. These can be attributed to the use of the approximate analytical formulae for the production profile. Finally, we summarize in Sec. X.

An important improvement of the current work over Refs. [11,13] is that the overall normalization of distortions is incorporated. The earlier works explicitly avoided this issue by considering ratios that eliminated the normalization factor. Our current simulations are now relatively accurate in absolute terms. At all times, the numbers of excess e, μ, and τ neutrinos per cubic volume are specified to within about 25%. The uncertainties are dominated by systematic effects, discussed in Sec. VI.

Throughout this paper, we work in units with $k = \hbar = c = 1$. The values of various parameters used in our current work, e.g., the baryon-to-photon ratio η, coincide with those of Ref. [13]. It is assumed that the chemical potentials for neutrinos are zero, so that the total number of neutrinos and antineutrinos is the same.

II. PURE PRODUCTION FOR THREE FLAVORS

Under the assumption that neutrinos are massless or do not mix, the distortion of the neutrino Fermi-Dirac distribution induced by the combination of neutrino thermal decoupling and e^+-e^- annihilation has been determined in Ref. [15] using the Boltzmann equation in an expanding FRW cosmology. For this situation, the distortions in the μ-neutrino and τ-neutrino distributions are equal, as are the distortions for antineutrinos and neutrinos of the same flavor. However, in the presence of mixing and neutrino oscillations, these equalities do not hold, and it is necessary to generalize the results of Ref. [15]. The purpose of this section is to obtain the generalized equations.

We begin by listing four of the more important approximations made in the analysis. First, at the energies and temperatures of interest, the difference between Fermi-Dirac and Maxwell-Boltzmann statistics is unimportant because there is little fermion degeneracy. For calculational purposes it is convenient to use Maxwell-Boltzmann statistics. A second approximation is the restriction to dominant weak-interaction effects, of order G_F^2. This is an excellent approximation during the time interval of interest in the early Universe.

A third approximation concerns the value of

$$\delta(t) \equiv T_\gamma/T - 1 \ , \tag{2.1}$$

where T_γ is the photon temperature and T is the neutrino temperature. The quantity $\delta(t)$ is a measure of the photon-neutrino temperature difference $T_\gamma - T$, to

which the distortions of the neutrino distributions are proportional. An exact computation of $\delta(t)$ is infeasible. However, it may be approximated by $\delta_0(t)$, where $\delta_0(t)$ is obtained assuming that neutrinos are always thermally decoupled and that they do not share in the heat released by e^+-e^- annihilations. While this approximation is poor for early times when the temperature is above ~ 5 MeV, the corresponding values of $\delta(t)$ are relatively small, and so the error introduced in the distortion is minimal. A correction to $\delta_0(t)$ partially compensating for the approximation is given in Ref. [15].

A fourth approximation is to set the electron mass m_e to zero. This is particularly convenient when computing scattering amplitudes. The approximation is reasonable for $T \gtrsim 0.5$ MeV. It does not introduce a large error for $T < 0.5$ MeV because most of the production occurs at temperatures above 0.5 MeV.

We next introduce the neutrino distortions. When neutrinos are in thermal equilibrium, their energy distribution is governed by the Maxwell-Boltzmann factor $f_0(E)$ given by

$$f_0(E) = \exp\left(-\frac{E}{T}\right) , \tag{2.2}$$

where E is the neutrino energy. As T drops below about 5 MeV, neutrinos decouple thermally. The distribution $f_{\nu_f}(E,t)$ for each neutrino ν_f of flavor f, $\nu_f = \nu_e$, ν_μ, ν_τ, $\bar{\nu}_e$, $\bar{\nu}_\mu$ or $\bar{\nu}_\tau$, then deviates from the Maxwell-Boltzmann one. We write

$$f_{\nu_f}(E,t) = f_0(E) + \Delta_{\nu_f}(E,t) . \tag{2.3}$$

This equation defines the distortions $\Delta_{\nu_f}(E,t)$.

For early times t when the system is hot, $\Delta_{\nu_f}(E,t) = 0$, $f_{\nu_f}(E) = f_0(E)$ and there is no deviation from standard statistics. For later times, $\Delta_{\nu_f}(E,t)$ is nonzero but small compared to $f_0(E)$ because the neutrinos are weakly interacting and are only mildly sensitive to the reheating from e^+-e^- annihilation. Thus, $\Delta_{\nu_f}(E,t)$ can be treated as a perturbation. Since electron neutrinos are somewhat more sensitive to e^+-e^- annihilation than μ or τ neutrinos, Δ_{ν_e} is larger than Δ_{ν_μ} or Δ_{ν_τ}.

The procedure for obtaining equations for the Δ_{ν_f} is given in Ref. [15]. We therefore restrict ourselves here to outlining our derivation of the generalized equations for the distortions. Note that, throughout the calculations, each neutrino momentum p and energy E can be equated. This is an excellent approximation since the neutrinos are ultra-relativistic at the temperatures of interest. Also, in working with the Boltzmann equation for $f_{\nu_f}(E)$ in an expanding Universe, it is convenient to use the variable E/T whenever possible since, for relativistic particles, it does not redshift as the Universe expands. The FRW scale factor $R(t)$ evolves to maintain $T(t)R(t)$ constant to a good approximation because neutrinos are decoupling and do not participate heavily in the e^+-e^- reheating. In contrast, the photon temperature T_γ rises relative to T during e^+-e^- annihilations.

The squared matrix elements of neutrino-scattering processes appear in the Boltzmann equation. There are 42 different basic processes:

$$\begin{gathered}
\nu_a + \bar{\nu}_a \to e^+ + e^-, \quad \nu_a + \bar{\nu}_a \to \nu_b + \bar{\nu}_b , \\
\nu_a + e^- \to \nu_a + e^-, \quad \bar{\nu}_a + e^- \to \bar{\nu}_a + e^- , \\
\nu_a + e^+ \to \nu_a + e^+, \quad \bar{\nu}_a + e^+ \to \bar{\nu}_a + e^+ , \\
\nu_a + \nu_b \to \nu_a + \nu_b, \quad \bar{\nu}_a + \bar{\nu}_b \to \bar{\nu}_a + \bar{\nu}_b , \\
\nu_a + \bar{\nu}_b \to \nu_a + \bar{\nu}_b, \quad a \neq b ,
\end{gathered} \tag{2.4}$$

where a and b stand for e, μ, or τ. In the Boltzmann equation, an initial neutrino is distinguished. This leads to 24 additional cases. Thus, there are a total of 66 distinguished-neutrino processes. For each particular neutrino or antineutrino, there are 11 cases.

In the calculation, hard scattering of neutrinos off nucleons can be neglected because the nucleon density is small. Also, nucleons do not affect neutrino oscillations through forward scattering because electron and muon neutrinos are scattered in the same way. As noted above, processes involving electrons and neutrinos participate more in the reheating due to charged-current interactions from $W^\pm$ exchange. In contrast, pure neutrino and antineutrino processes tend to equilibriate the distributions.

The electron and positron Maxwell-Boltzmann distributions are

$$f_{e^\pm}(E_e,t) = \exp\left(-\frac{E_e}{T_\gamma}\right) . \tag{2.5}$$

Since the electron mass is set to zero, $E_e = p_e$. Expressing Eq. (2.5) in terms of the neutrino temperature T and the fractional temperature difference $\delta(t)$ gives

$$f_{e^\pm}(p_e,t) = f_0(p_e)\left(1 + \frac{p_e}{T}\delta(t) + \cdots\right) . \tag{2.6}$$

The Boltzmann equation itself and the squared matrix elements for all the processes in Eq. (2.4) are given in Ref. [15]. To obtain equations for the distortions, Eqs. (2.3) and (2.6) and the squared matrix elements are substituted into the Boltzmann equation, and an expansion is performed in powers of Δ_{ν_a}, $\Delta_{\bar{\nu}_a}$, and $\delta(t)$. The term linear in these quantities provides differential equations for the Δ_{ν_f}. For calculational purposes, it is useful to consider the distortions Δ_{ν_f} and other quantities as functions of E/T and t, rather than E and t.

The resulting differential equations can be simplified by performing many of the phase space integrations. After some calculation, we obtain for the six distortions Δ_{ν_f} a set of six linear coupled differential equations, given by

$$\frac{d\Delta_{\nu_f}}{dt}\left(\frac{E}{T},t\right)=\frac{4G_F^2T^5}{\pi^3}\left[-A_{\nu_f}\left(\frac{E}{T}\right)\Delta_{\nu_f}\left(\frac{E}{T},t\right)+B_{\nu_f}\left(\frac{E}{T}\right)\delta(t)+\sum_{\nu_{f'}}\int_0^\infty\frac{dE'}{T}C_{\nu_f\nu_{f'}}\left(\frac{E}{T},\frac{E'}{T}\right)\Delta_{\nu_{f'}}\left(\frac{E'}{T},t\right)\right] , \tag{2.7}$$

where the A, B, and C coefficients are determined. They are presented in Appendix A.

Since $A_{\nu_f}>0$, the A terms induce damping. The B terms induce reheating of neutrinos, arising from interactions with positrons and electrons. Note that our conventions for the A and B coefficients differ from Ref. [15] by a factor of $E/(T\pi^3)$, included here as part of the overall normalization constant in Eq. (2.7). The C terms represent the coupling of neutrinos of different energies. This is the origin of the integration over the final state neutrino energy E'. Note that all the coefficients are independent of t, since they are functions only of E/T and E'/T.

We remark that Eqs. (2.7) correctly reduce to the corresponding equations[1] of Ref. [15] in the limits

$$\Delta_{\bar{\nu}_e}\to\Delta_{\nu_e},\quad \Delta_{\nu_\tau}\to\Delta_{\nu_\mu},\quad \Delta_{\bar{\nu}_\mu}\to\Delta_{\nu_\mu},\quad \Delta_{\bar{\nu}_\tau}\to\Delta_{\nu_\mu} . \tag{2.8}$$

III. PURE OSCILLATIONS FOR TWO FLAVORS

In this section, we summarize the formalism of our earlier work for treating neutrino oscillations in the early Universe. We consider oscillations between two flavors ν_e and ν_μ.

The most convenient formulation uses the three-component vectors

$$\vec{v}(E,t)\equiv(\nu_e^\dagger\nu_e-\nu_\mu^\dagger\nu_\mu,2\,\mathrm{Re}(\nu_e^\dagger\nu_\mu),2\,\mathrm{Im}(\nu_e^\dagger\nu_\mu)) , \tag{3.1}$$
$$\vec{w}(E,t)\equiv(\bar{\nu}_e^\dagger\bar{\nu}_e-\bar{\nu}_\mu^\dagger\bar{\nu}_\mu,2\,\mathrm{Re}(\bar{\nu}_e^\dagger\bar{\nu}_\mu),2\,\mathrm{Im}(\bar{\nu}_e^\dagger\bar{\nu}_\mu)) ,$$

where ν_f and $\bar{\nu}_f$ are fields for neutrinos and antineutrinos of flavor f, respectively. We use the normalization convention that $\nu_f^\dagger\nu_f(E)$ is the number of neutrinos of flavor f with energy E in a comoving volume of volume a^3 per unit E/T. The scaling factor a can be chosen arbitrarily. It increases with the redshift scale $R(t)$ as the Universe expands.

The oscillations equations resemble the motion of a particle in a magnetic field:

$$\frac{\partial\vec{v}(E)}{\partial t}=\vec{v}(E)\times\vec{B}_v(E) , \tag{3.2}$$
$$\frac{\partial\vec{w}(E)}{\partial t}=\vec{w}(E)\times\vec{B}_w(E) ,$$

where the effective magnetic fields are

$$\vec{B}_v(E,t)=\frac{\vec{\Delta}}{2E}-\vec{V}_{\nu\nu}-(V_{CP+}(E)+V_{CP-})\hat{e}_1 , \tag{3.3}$$
$$\vec{B}_w(E,t)=\frac{\vec{\Delta}}{2E}+\vec{V}_{\nu\nu}^*-(V_{CP+}(E)-V_{CP-})\hat{e}_1 .$$

The next few paragraphs explain the terms in Eq. (3.3).

Vacuum oscillations are produced by the term $\vec{\Delta}/(2E)$, where

$$\vec{\Delta}=\Delta(\cos2\theta,-\sin2\theta,0) . \tag{3.4}$$

Here, θ is the vacuum mixing angle and Δ is the mass-squared difference of vacuum-mass-eigenstate neutrinos: $\Delta=m_2^2-m_1^2$. For pure vacuum oscillations, neutrinos are in mass eigenstates when $\vec{v}$ and $\vec{\Delta}$ are aligned.

The interaction of neutrinos with background electrons and positrons is governed by two potentials, V_{CP+} and V_{CP-}, where V_{CP+} is CP conserving and V_{CP-} is CP violating:

$$V_{CP+}(E,t)=-2\sqrt{2}G_FE(\rho_{e^-}+p_{e^-}+\rho_{e^+}+p_{e^+})/M_W^2 , \tag{3.5}$$
$$V_{CP-}(t)=\sqrt{2}G_F(n_{e^-}-n_{e^+}) ,$$

where n_f, ρ_f, and p_f are respectively the number density, the energy density and the pressure of the charged lepton f. As the Universe expands, these quantities decrease. The effective magnetic fields associated with V_{CP+} and V_{CP-} are aligned along the one-axis fixed as $\hat{e}_1=(1,0,0)$. When neutrinos are in pure flavor eigenstates, the $\vec{v}$ are aligned with $\hat{e}_1$.

Finally, $\vec{V}_{\nu\nu}$ provides the neutrino-neutrino interactions. It is given by

$$\vec{V}_{\nu\nu}(t)=\frac{\sqrt{2}G_F}{a^3}(\langle\vec{v}\rangle-\langle\vec{w}^*\rangle) , \tag{3.6}$$

where

$$\langle\vec{v}(t)\rangle=\int_0^\infty\frac{dE}{T}\vec{v}(E,t) , \tag{3.7}$$
$$\langle\vec{w}(t)\rangle=\int_0^\infty\frac{dE}{T}\vec{w}(E,t) .$$

The asterisk in Eqs. (3.3) and (3.6) indicates that the sign of the third component of a vector is reversed, e.g., $(w_1,w_2,w_3)^*=(w_1,w_2,-w_3)$. Since $\vec{V}_{\nu\nu}$ renders the oscillation equations in Eq. (3.2) nonlinear, we often refer to it as the *nonlinear term.*

[1]Note that the factor $(c+8)$ in Eq. (2.11d) of Ref. [15] should be $(c+7)$, and the factor $(b+c+14)$ in Eq. (2.14b) should be $(b+c+13)$.

IV. SUMMARY OF RESULTS FOR PURE NEUTRINO OSCILLATIONS

For purposes of comparison with the new results given in the present paper, this section provides a summary of the main features of neutrino behavior in the early Universe described in Refs. [11,13]. Numerical solution of Eq. (3.2) for $\Delta > 0$ and $0 < \theta < \pi/4$ reveals that neutrino oscillations exhibit a number of effects, all attributable to the nonlinear neutrino-neutrino interaction term.

One feature of the neutrino behavior is its remarkable smoothness. As the Universe expands, the four interaction terms in Eq. (3.3) change. In the absence of the nonlinear term, the changes induce temporary oscillatory behavior. However, when the nonlinear term is present, no oscillations are observed.

Another feature of the behavior concerns decoherence. Without the nonlinear term, decoherence is a collective effect due to the different oscillation times of individual neutrinos. Individual neutrinos nonetheless undergo oscillatory behavior. In contrast, when the nonlinear term is present, individual neutrino vectors are approximately aligned and so do not exhibit independent oscillatory behavior.

A third feature of the nonlinear system is that individual neutrinos maintain themselves in configurations that are approximate nonlinear mass eigenstates (ANME). An instantantaneous nonlinear mass eigenstate diagonalizes the Hamiltonian at a given time. This occurs for an individual neutrino when its vector and magnetic field point in the same direction, so the right-hand side of Eq. (3.2) vanishes and the change in flavor content is momentarily zero. As the Universe expands, magnetic fields evolve. The ANME property means that a neutrino vector tends to follow changes in the associated magnetic field. It can be shown that alignment is a consequence of the ANME property and the dominance of the neutrino-neutrino interaction.

A fourth feature of neutrino behavior is CP suppression. Although CP-violating interactions are present, the buildup of asymmetry between neutrinos and antineutrinos is several magnitudes smaller than in the absence of the nonlinear neutrino-neutrino interactions. The CP-suppression mechanism can also be understood as a consequence of the ANME property. It involves a partial cancellation between the CP-asymmetric electron-neutrino and neutrino-neutrino interactions. This cancellation can be used to develop an analytical approximation scheme for the average and individual neutrino vectors. The scheme reproduces individual neutrino vectors to a few percent and the average vector to better than one percent.

The neutrino behavior also exhibits planarity, i.e., the third components of neutrino vectors are much smaller than the first and second components. In a linear system for which decoherence has set in, planarity holds for the average vector but not for individual neutrino vectors. Since instantaneous nonlinear mass eigenstates have zero third components, the ANME property implies that the third components of individual vectors are also small for the full nonlinear system.

Since the third components are small, it is tempting to conclude that they are unimportant. This is false. Disregarding them, which is equivalent to disregarding the imaginary part of the off-diagonal flavor term, in a poor approximation. While the first two components cancel to a large extent in the nonlinear term of Eq. (3.6), the third components tend to add because of the asterisk operation. Numerically, we find the third component of $\vec{V}_{\nu\nu}$ is of the same order of magnitude as the first two components.

Another feature of the neutrino behavior can be traced directly to the third component of $\vec{V}_{\nu\nu}$. When $\Delta < 10^{-9}$ eV^2, ANME configurations initially point approximately along the one-axis. As the Universe expands and energies redshift, the vacuum term grows, becoming dominant some tens of seconds later. The magnetic fields then point toward $\vec{\Delta}$, so ANME configurations are close to vacuum-mass eigenstates. Surprisingly, however, the neutrino vectors rotate toward vacuum-mass eigenstates earlier than expected. This effect, called precocious rotation, arises because a negative contribution develops to the third component of $\vec{V}_{\nu\nu}$, which causes a rotation of the neutrino vectors in the 1-2 plane.

In passing, we mention two other effects involving the imaginary part of the off-diagonal flavor term, arising in the $\Delta < 0$ parameter region [12]. First, there exists a flavor-conversion mechanism that is completely different from the Mikheyev-Smirnov-Wolfenstein (MSW) effect [20]. It is efficient and occurs even for very small mixing angles. The second effect, called self-maintained coherence, is a collective mode of the nonlinear system in which a large fraction of neutrinos oscillate in unison. The effect in the pure neutrino gas [19] differs from that in the mixed neutrino-antineutrino gas [13,21], where the third component of $\vec{V}_{\nu\nu}$ plays an important role.

V. EQUATIONS FOR COMBINED PRODUCTION AND OSCILLATIONS

If neutrino masses and mixings are nonzero, neutrino oscillations begin as distortions develop in the neutrino distributions. In principle, the oscillations could significantly affect the flavor content when the photon reheating and neutrino decoupling are complete. For large mixing angle, for instance, any excess electron neutrinos produced could oscillate into muon neutrinos, potentially producing a muon-neutrino excess that in the absence of oscillations would not arise. Furthermore, any change in flavor content due to oscillations affects the rates of the scattering processes in the Boltzmann equation. The goal of this section is to obtain equations governing the production of nonequilibrium distributions when neutrino mixing is present.

During an infinitesimal time interval, the change in the neutrino distributions is due to the change created by the Boltzmann equation plus the change due to neutrino oscillations. Hence, it suffices to add the contributions from pure production and from pure oscillations. This involves combining the equations in Secs. II and III. However, the

formulae in Sec. II are expressed in a different basis from those in Sec. III. For numerical purposes, we elect to use the vector-type variables of Sec. III. We therefore begin this section by rewriting the pure-production equations of Sec. II.

The first step in this process is to relate the distortions Δ_{ν_f} to the density like variables $\nu_f^\dagger \nu_f$. The connection is given by

$$\Delta_{\nu_f}(E,t)\frac{(aT)^3}{2\pi^2}\left(\frac{E}{T}\right)^2 = \nu_f^\dagger \nu_f(E,t)\ . \tag{5.1}$$

Note that the factor $E^2a^3T/(2\pi^2)$ is independent of time. Multiplying both sides of Eq. (2.7) by this factor leads to the reformulation of the pure-production equations as

$$\frac{\partial \nu_f^\dagger \nu_f}{\partial t}(E,t) = \frac{4G_F^2T^5}{\pi^3}\left(- A_{\nu_f}\left(\frac{E}{T}\right)\nu_f^\dagger\nu_f(E,t) + \tilde{B}_{\nu_f}\left(\frac{E}{T}\right)\delta(t) + \sum_{\nu_{f'}}\int_0^\infty \frac{dE'}{T}\tilde{C}_{\nu_f\nu_{f'}}\left(\frac{E}{T},\frac{E'}{T}\right)\nu_{f'}^\dagger\nu_{f'}(E',t)\right), \tag{5.2}$$

where the coefficients with tildes are defined by

$$\begin{aligned}\tilde{B}_{\nu_f}\left(\frac{E}{T}\right) &\equiv B_{\nu_f}\frac{(aT)^3}{2\pi^2}\left(\frac{E}{T}\right)^2\ ,\\ \tilde{C}_{\nu_f\nu_{f'}}\left(\frac{E}{T},\frac{E'}{T}\right) &\equiv \frac{E^2}{E'^2}C_{\nu_f\nu_{f'}}\left(\frac{E}{T},\frac{E'}{T}\right)\ .\end{aligned} \tag{5.3}$$

The A coefficients remain unchanged. Since a^3T^3 is time independent, so is $\tilde{B}_{\nu_f}\left(\frac{E}{T}\right)$.

The second step is to convert to the vector formulation. To accompany the 1, 2, and 3 neutrino-vector components specified in Sec. III, we define new 0 and 4 components by

$$v_0\left(\frac{E}{T},t\right) \equiv (\nu_e^\dagger\nu_e + \nu_\mu^\dagger\nu_\mu)(E,t),\quad v_4\left(\frac{E}{T},t\right) \equiv \nu_\tau^\dagger\nu_\tau(E,t)\ . \tag{5.4}$$

and

$$w_{\bar{0}}\left(\frac{E}{T},t\right) \equiv (\bar{\nu}_e^\dagger\bar{\nu}_e + \bar{\nu}_\mu^\dagger\bar{\nu}_\mu)(E,t),\quad w_{\bar{4}}\left(\frac{E}{T},t\right) \equiv \bar{\nu}_\tau^\dagger\bar{\nu}_\tau(E,t)\ . \tag{5.5}$$

Here and henceforth, we use a bar over a neutrino-vector index to help distinguish neutrinos from antineutrinos. Also, to render the variable dependence the same for production and oscillations, we use the arguments E/T and t instead of E and t for the new components v_0, v_4, $w_{\bar{0}}$, and $w_{\bar{4}}$. The zero component v_0 is associated with the ν_e-ν_μ excess in the canonical comoving volume, while the fourth component v_4 is the ν_τ excess in this volume. Corresponding statements hold for the antineutrinos.

When reexpressed in vector notation, Eq. (2.7) for pure production becomes

$$\begin{aligned}\frac{\partial v_a}{\partial t}\left(\frac{E}{T},t\right) = \frac{4G_F^2T^5}{\pi^3}\Bigg(&- \sum_b A_{ab}\left(\frac{E}{T}\right)v_b\left(\frac{E}{T},t\right) + B_a\left(\frac{E}{T}\right)\delta(t)\\ &+ \sum_b\int_0^\infty\frac{dE'}{T}C_{ab}\left(\frac{E}{T},\frac{E'}{T}\right)v_b\left(\frac{E'}{T},t\right) + \sum_{\bar{b}}\int_0^\infty\frac{dE'}{T}C_{a\bar{b}}\left(\frac{E}{T},\frac{E'}{T}\right)w_{\bar{b}}\left(\frac{E'}{T},t\right)\Bigg),\end{aligned} \tag{5.6}$$

where $a = 0$, 1, or 3, $b = 0$, 1, or 3, and $\bar{b} = \bar{0}$, $\bar{1}$, or $\bar{3}$. The new coefficients A_{ab}, B_a, C_{ab}, and $C_{a\bar{b}}$ in this equation are linear combinations of the previously defined coefficients A_{ν_f}, $\tilde{B}_{\nu_f}$, and $\tilde{C}_{\nu_f\nu'_f}$. They are given in Appendix B. The new coefficients are functions of neutrino energy and temperature, but again only in the combinations E/T and E'/T. They appear due to the change of basis from the vectors $\vec{e}_1$ and $\vec{e}_2$ to the vectors $\vec{e}_1 + \vec{e}_2$ and $\vec{e}_1 - \vec{e}_2$.

A similar derivation holds for antineutrinos, yielding

$$\begin{aligned}\frac{\partial w_{\bar{a}}}{\partial t}\left(\frac{E}{T},t\right) = \frac{4G_F^2T^5}{\pi^3}\Bigg(&- \sum_{\bar{b}} A_{\bar{a}\bar{b}}\left(\frac{E}{T}\right)w_{\bar{b}}\left(\frac{E}{T},t\right) + B_{\bar{a}}\left(\frac{E}{T}\right)\delta(t) + \sum_b\int_0^\infty\frac{dE'}{T}C_{\bar{a}b}\left(\frac{E}{T},\frac{E'}{T}\right)v_b\left(\frac{E'}{T},t\right)\\ &+ \sum_{\bar{b}}\int_0^\infty\frac{dE'}{T}C_{\bar{a}\bar{b}}\left(\frac{E}{T},\frac{E'}{T}\right)w_{\bar{b}}\left(\frac{E'}{T},t\right)\Bigg).\end{aligned} \tag{5.7}$$

The coefficients $A_{\bar{a}\bar{b}}$, $B_{\bar{a}}, C_{\bar{a}b}$, and $C_{\bar{a}\bar{b}}$ are also provided in Appendix B. Note that if the first index of a coefficient is unbarred then it enters in a neutrino equation. If instead the first index is barred, then the coefficient enters in an antineutrino equation. Equations (5.6) and (5.7) complete the change of basis to vector notation for the pure-production case discussed in Sec. II.

The equations for the combined system with simultaneous production and oscillations follow from the above analysis. For neutrinos, adding the right-hand sides of Eqs. (3.2) and (5.6) gives

$$\frac{\partial v_a}{\partial t}\left(\frac{E}{T},t\right) = \left[\vec{v}\left(\frac{E}{T},t\right)\times\vec{B}_v\right]_a + \frac{4G_F^2T^5}{\pi^3}\left[-\sum_b A_{ab}\left(\frac{E}{T}\right)v_b\left(\frac{E}{T},t\right) + B_a\left(\frac{E}{T}\right)\delta(t) + \sum_b\int_0^\infty \frac{dE'}{T}C_{ab}\left(\frac{E}{T},\frac{E'}{T}\right)v_b\left(\frac{E'}{T},t\right) + \sum_{\bar{b}}\int_0^\infty \frac{dE'}{T}C_{a\bar{b}}\left(\frac{E}{T},\frac{E'}{T}\right)w_{\bar{b}}\left(\frac{E'}{T},t\right)\right] . \tag{5.8}$$

For antineutrinos, adding the right-hand sides of Eqs. (3.2) and (5.7) gives

$$\frac{\partial w_{\bar{a}}}{\partial t}\left(\frac{E}{T},t\right) = \left[\vec{w}\left(\frac{E}{T},t\right)\times\vec{B}_w\right]_{\bar{a}} + \frac{4G_F^2T^5}{\pi^3}\left[-\sum_{\bar{b}} A_{\bar{a}\bar{b}}\left(\frac{E}{T}\right)w_{\bar{b}}\left(\frac{E}{T},t\right) + B_{\bar{a}}\left(\frac{E}{T}\right)\delta(t) \times\sum_b\int_0^\infty \frac{dE'}{T}C_{\bar{a}b}\left(\frac{E}{T},\frac{E'}{T}\right)v_b\left(\frac{E'}{T},t\right) + \sum_{\bar{b}}\int_0^\infty \frac{dE'}{T}C_{\bar{a}\bar{b}}\left(\frac{E}{T},\frac{E'}{T}\right)w_{\bar{b}}\left(\frac{E'}{T},t\right)\right] . \tag{5.9}$$

Equations (5.8) and (5.9) are the desired equations. Note that in Eqs. (5.8) and (5.9) we define

$$[\vec{v}(E)\times\vec{B}_v]_a \equiv 0 \quad \text{for } a = 0 \text{ and } 4 ,$$

$$[\vec{w}(E)\times\vec{B}_w]_{\bar{a}} \equiv 0 \quad \text{for } \bar{a} = 0 \text{ and } 4 . \tag{5.10}$$

The 1, 2, and 3 components are computed normally.

VI. TECHNICAL ISSUES AND NUMERICAL METHODOLOGY

In this section, we first describe the discretization of Eqs. (5.8) and (5.9). We next present some analytical results for the resulting equations and discuss the implementation of the approximation for $\delta(t)$, already mentioned in Sec. II, along with a method for partially compensating the approximation of zero electron and positron mass. Finally, we present some details about the algorithm used and the range of data obtained.

Numerical solution of Eqs. (5.8) and (5.9) requires conversion of the continuous energy variable to a discrete one. We allow E/T to vary from $(E/T)_{\min}$ to $(E/T)_{\max}$ and divide this interval into N_E bins of equal spacing. Indices j and k ranging from 1 to N_E are used to label quantities associated with neutrino and antineutrino energy bins, respectively. Most simulations were performed with $(E/T)_{\min} = 0.1$, $(E/T)_{\max} = 20.0$, and $N_E = 61$.

We define discrete densitylike variables associated with the jth and kth bins by

$$\nu_f^{j\dagger}\nu_{f'}^j = \nu_f^\dagger\nu_{f'}(E^j)\frac{\Delta E^j}{T}, \quad \bar{\nu}_f^{k\dagger}\bar{\nu}_{f'}^k = \bar{\nu}_f^\dagger\bar{\nu}_{f'}(E^k)\frac{\Delta E^k}{T} . \tag{6.1}$$

With this definition, $\nu_f^{j\dagger}\nu_f^j$ represents the number of neutrinos of flavor f with energies between E^j and $E^j+\Delta E^j$ in the canonical comoving volume $a^3(t)$, while $\bar{\nu}_f^{k\dagger}\bar{\nu}_f^k$ is the number of antineutrinos of flavor f in the kth energy bin in the volume $a^3(t)$. Discrete neutrino and antineutrino vectors associated with the jth and kth bins can similarly be introduced, via

$$v_a^j(t) \equiv \frac{\Delta E^j}{T}v_a\left(\frac{E}{T},t\right), \quad w_{\bar{a}}^k(t) \equiv \frac{\Delta E^k}{T}w_{\bar{a}}\left(\frac{E}{T},t\right) . \tag{6.2}$$

Differential equations for v_a^j can be obtained by multiplication of Eq. (5.8) with $\Delta E^j/T$ and replacement of the continuous integral over E'/T by a discrete sum. Since $\Delta E^j/T$ is time independent, it can be moved inside the time derivative on the left-hand side. For antineutrinos a similar procedure is performed to give equations for $w_{\bar{a}}^k$. The resulting discrete equations resemble the continuum equations (5.8) and (5.9) with the identifications

$$E\to E^i, \quad E'\to E^m, \quad \int_0^\infty\frac{dE'}{T}\to\sum_m ,$$

$$v_a\left(\frac{E^j}{T},t\right)\to v_a^j(t), \quad w_{\bar{a}}\left(\frac{E^k}{T},t\right)\to w_{\bar{a}}^k(t) ,$$

$$A_{cd}\left(\frac{E}{T}\right) \to A^i_{cd} \equiv A_{cd}\left(\frac{E^i}{T}\right) ,$$

$$B_c\left(\frac{E}{T}\right) \to B^i_c \equiv \frac{\Delta E^i}{T} B_c\left(\frac{E^i}{T}\right) ,$$

$$C_{cd}\left(\frac{E}{T},\frac{E'}{T}\right) \to C^{im}_{cd} \equiv \frac{\Delta E^i}{\Delta E^m} C_{cd}\left(\frac{E^i}{T},\frac{E^m}{T}\right) ,$$

$$\vec{B}_v(E,t) \to \vec{B}^i_v(t) \equiv \vec{B}_v(E^i,t), \quad \vec{B}_w(E,t) \to \vec{B}^i_w(t) \equiv \vec{B}_w(E^i,t) ,$$

$$V_{CP^+}(E) \to V^i_{CP^+} \equiv V_{CP^+}(E^i) \text{ in } \vec{B}_v \text{ and } \vec{B}_w \text{ of Eq. (3.3)} ,$$

$$\langle v_a(t)\rangle \to \sum_j v^j_a(t), \quad \langle w_{\bar{b}}(t)\rangle \to \sum_k w^k_{\bar{b}}(t) \text{ in } \vec{V}_{\nu\nu} \text{ of Eq. (3.6)} , \tag{6.3}$$

where the label c can be a or $\bar{a}$ and d can be b or $\bar{b}$, and where the indices i and m stand for j or k.

In the absence of production, i.e., setting $A^i_{cd} = B^i_c = C^{im}_{cd} = 0$, the equations reduce to those in Refs. [11,13] for pure oscillations. In the absence of oscillations, i.e., $\vec{B}_v = \vec{B}_w = 0$, the discrete set of differential equations can be analytically integrated, as we show next.

The first step is to convert the time-integration variable t to the neutrino temperature T, via

$$T = \frac{1}{(2\kappa_0 t)^{1/2}}, \quad \frac{dT}{dt} = -\kappa_0 T^3 , \tag{6.4}$$

where

$$\kappa_0 \equiv \left(\frac{4\pi^3 G_N g_*}{45}\right)^{1/2} . \tag{6.5}$$

Here, G_N is Newton's constant and g_* counts the total number of effectively massless degrees of freedom. For $T > 1$ MeV, $g_* = 10.75$.

The structure of the discrete version of Eqs. (5.8) and (5.9) or of Eq. (2.7) then becomes

$$\frac{dx_r(T)}{dT} = -k_0 T^2 [\mathcal{B}_r \delta(T) + \mathcal{C}_{rs} x_s(T)] , \tag{6.6}$$

where $\mathcal{B}$ is related to the B coefficients and $\mathcal{C}$ contains both C and A coefficients. Note that both the sets of coefficients $\mathcal{B}$ and $\mathcal{C}$ are independent of time and temperature. In Eq. (6.6),

$$k_0 \equiv \frac{4G_F^2}{\kappa_0 \pi^3} , \tag{6.7}$$

and r, s represent both flavor and energy-binning indices: $r \leftrightarrow c, i$ with c ranging over six values and i ranging from 1 to N_E. In the formulation of Eqs. (5.8) and (5.9), x represents either v or $\bar{w}$, and c ranges over 0,1,4,$\bar{0}$, $\bar{1}$, $\bar{4}$. For the formulation of Eq. (2.7), x represents one of the six distortions Δ_{ν_f} and c ranges over $\nu_e, \nu_\mu, \nu_\tau, \bar{\nu}_e, \bar{\nu}_\mu, \bar{\nu}_\tau$. The solution to Eq. (6.6) is

$$x_r(T) = k_0 \int_T^\infty d\bar{T}\, \bar{T}^2 \delta(\bar{T}) \left[\exp\left(\frac{k_0}{3}(\bar{T}^3 - T^3)\mathcal{C}\right)\right]_{rs} \mathcal{B}_s . \tag{6.8}$$

Although the $6N_E \times 6N_E$ matrix $\mathcal{C}$ is not symmetric, it does have a complete set of right eigenvectors $v^{(q)}$ defined by

$$\mathcal{C} v^{(q)} = \lambda^{(q)} v^{(q)} , \tag{6.9}$$

where $q = 1, \ldots, 6N_E$. The $\lambda^{(q)}$ are the right eigenvalues of $\mathcal{C}$. The $v^{(q)}$ are not orthogonal but they are complete. Thus, the vector $\mathcal{B}$ can be expanded in terms of the $v^{(q)}$ using

$$\mathcal{B} = \sum_q \beta_{(q)} v^{(q)} , \tag{6.10}$$

where the $\beta_{(q)}$ are expansion coefficients. The solution (6.9) becomes

$$x_r(T) = k_0 \sum_q \beta_{(q)} v^{(q)}_r \int_T^\infty d\bar{T}\, \bar{T}^2 \delta(\bar{T}) \times \exp\left[\frac{k_0}{3}(\bar{T}^3 - T^3)\lambda^{(q)}\right] . \tag{6.11}$$

Equation (6.11) provides an efficient way to obtain results for the pure-production case. The integrals in (6.11) can be computed rapidly by various methods. One needs $\mathrm{Re}\lambda^{(q)} < 0$ for convergence. For different values of N_E, we have computed the right eigenvalues of $\mathcal{C}$ and verified convergence for sufficiently large N_E. This analysis aided our determination of the minimum size of N_E necessary for numerically accurate results. As a side remark, we note that a reasonable approximation to pure production can be obtained by saturating the sum in Eq. (6.11)

with terms corresponding to those eigenvalues with the largest real parts.

To integrate the distortion equations, a formula for $\delta(t)$ is needed. We follow Ref. [15] and approximate $\delta(t)$ by $\delta_0(t)$, given by

$$\delta_0(t) = \left(\frac{12}{4 + z^3 K_1(z) + 4z^2 K_2(z)}\right)^{1/3} - 1 , \quad (6.12)$$

where $z = m_e/T_\gamma$ and $K_1(z)$ and $K_2(z)$ are modified Bessel functions. Recall that $\delta_0(t)$ is obtained under the assumption that neutrinos are thermally decoupled for all times.

The direct use of Eq. (6.12) for arbitrarily early times leads to an inconsistency. It implies an early-time behavior

$$\delta_0(t) \approx \frac{1}{36}\left(\frac{m_e}{T}\right)^2 , \quad (6.13)$$

for $T \gg m_e$. If this expression were used in the pure-production equations, one would find that the early-time behavior of $\Delta_{\nu_f}\left(\frac{E}{T}, t\right)$ is

$$\Delta_{\nu_f}\left(\frac{E}{T}, t\right) \approx c_{\nu_f}\left(\frac{E}{T}\right)\left(\frac{1}{T}\right)^2 , \quad (6.14)$$

where $c_{\nu_f}\left(\frac{E}{T}\right)$ is a time-independent constant. Since the total excess density is obtained by multiplying by $E^2 dE/2\pi^2$ and integrating over E, it would follow that the excess density of electron neutrinos over muon neutrinos increases at earlier times. If this result were correct, it would pose a severe numerical difficulty. When both production and oscillations are treated, the neutrino-neutrino potential would be important for $T \lesssim 100$ MeV. This would necessitate starting the integration of Eqs. (5.8) and (5.9) at $T \sim 100$ MeV. To integrate over the large temperature range from ~ 100 MeV down to ~ 1 MeV would be prohibitive in computer time.

Fortunately, the early-time behavior in Eq. (6.13) is incorrect. The source of the difficulty is the assumption that neutrinos are thermally decoupled for all times. It must be true that for $T > 10$ MeV neutrinos are in thermal equilibrium with photons, so that δ is exponentially small. The results of Refs. [15] and [16] suggest that neutrinos decouple in the temperature range from 2 to 5 MeV. Higher-energy neutrinos decouple later, at a lower temperature. Also, e neutrinos decouple somewhat later than μ and τ neutrinos. In any case, it is evident that δ should be set to zero at sufficiently early times.

An exact formula for $\delta(t)$ is not available. Instead, we make the simple approximation

$$\delta(t) = \delta_0(t) \quad \text{for } t > t_s , \qquad \delta(t) = 0 \quad \text{for } t < t_s , \quad (6.15)$$

where t_s is a cutoff time. Numerically, t_s is the time at which we start the integration of Eqs. (5.8) and (5.9).

In principle, a better approximation can be made by taking t_s to be a function of bin energy. In other words, δ is set to zero earlier for low-energy neutrinos and later for high-energy neutrinos. If one is interested only in results for $t \gtrsim 0.3$ s, then the detailed manner in which δ is turned on is unimportant. For simplicity, we take t_s to be energy-bin independent. We denote by T_s the neutrino temperature at the time t_s.

The approximation (6.15) is a significant improvement over the use of δ_0 at all times. It is also better than incorporating the $\delta T_\gamma/T$ correction to δ provided in Ref. [15]. For numerical purposes, we take $T_s = 3.0$ MeV, corresponding to a starting time t_s of about 0.082 s. We have varied T_s somewhat and checked that final production results are relatively insensitive to this choice. Note that, although it is important to turn off δ for early times in dealing with neutrino oscillations, it is less important in the pure-production case if one is interested in results at late times. Hence, using the approximation δ_0 at all times is unlikely to affect the conclusions of Ref. [15] concerning the primordial ^{4}He abundance.

Another approximation made is to set the electron and positron mass to zero. When the temperature drops below 0.5 MeV, electrons and positrons quickly annihilate and production rapidly ceases. This is not correctly incorporated in the formulae for the scattering processes when $m_e = 0$ is used, so some error is made below 1 MeV. A simple way to compensate for this is to stop the production prematurely. We chose to terminate our numerical integrations involving production processes at the temperature $T_f = 0.75$ MeV, which corresponds to a time t_f of about 1.312 s. Beyond T_f, we proceed with integration of the pure oscillation equations (3.2) instead. Varying T_f from 0.9 to 0.5 MeV changes the distortion functions by about 20%. Hence, the 20% uncertainty in selecting T_f is the biggest uncertainty in our results.

To minimize the chances of programming errors, at all stages two independent programs were written and results were checked to double-precision machine accuracy. Desktop Hewlett-Packard and Sun work stations were used.

The numerical integrations were performed with a fourth-order Runge-Kutta algorithm applied to Eqs. (5.8) and (5.9). The scale factor $a(t)$ at $T_s = 3.0$ MeV was taken to be 0.5 MeV^{-1} to facilitate comparison with the results of Ref. [13]. The point is that when $T_s = 1.5$ MeV, $a(t)$ becomes 1.0 MeV^{-1}, which is the value selected in Ref. [13]. Since the A, B, and C coefficients are time independent, they could be computed once initially and stored in memory.

The integration combining production and oscillation proceeds about one-hundred times slower than pure oscillation integration due to the increased amount of arithmetic. For this reason, verification of all the runs in Ref. [13] was impractical. However, sufficiently many simulations were performed to confirm the conclusions of Ref. [13]. In addition to the situation without oscillations, we studied the cases $\sin^2 2\theta = 0.81$ with $\Delta = 10^{-12}$ eV^2, $\Delta = 10^{-9}$ eV^2, $\Delta = 10^{-7}$ eV^2, $\Delta = 10^{-6}$ eV^2, and $\Delta = 10^{-4}$ eV^2, and the cases $\sin^2 2\theta = 0.25$ with $\Delta = 10^{-12}$ eV^2, $\Delta = 10^{-9}$ eV^2, and $\Delta = 10^{-6}$ eV^2.

VII. RESULTS FOR PURE PRODUCTION WITHOUT OSCILLATIONS

For the case without flavor mixing, the improvements considered in Sec. VI lead to somewhat different nonequilibrium distortion profiles than those of Refs. [15,16]. This section presents our results and discusses these differences.

Figure 1 displays our final production profiles at $T_f = 0.75$ MeV for zero mixing angle. The curves plotted are $\nu_e^\dagger\nu_e(E)/T$, $\nu_\mu^\dagger\nu_\mu(E)/T$, their sum, and their difference, as functions of neutrino energy E. The continuous distortion densities $\nu_f^\dagger\nu_f(E)$ are defined in Eq. (5.1). We remind the reader that $\nu_f^\dagger\nu_f(E)\Delta E/T$ represents the excess number of neutrinos of flavor f between E and $E+\Delta E$ in the canonical comoving volume. Each curve therefore represents a neutrino excess per unit energy over the Maxwell-Boltzmann distribution in the volume a^3, and the area under a curve is the total excess in that volume.

The production profile for the τ neutrinos is identical to that for the μ neutrinos because, in the absence of mixing, the system is symmetric under the interchange of μ and τ flavors. Also, the distortions for antineutrinos are the same as for the corresponding neutrinos because the system is CP symmetric when $\theta = 0$.

The electron- and muon-neutrino curves are negative for small E, indicating a deficit of neutrinos in the low-energy region compared to the Maxwell-Boltzmann distribution. Physically, the effect arises from the reheating of neutrinos by e^+-e^- annihilation, which shifts some low-energy neutrinos to higher energies and thereby reduces the number in the low-energy region. As can be seen from Fig. 1, the deficit largely cancels in the neutrino-difference profile, which represents the difference between electron- and muon-neutrino number densities. The flavor-density nonequilibrium distortions peak at $E \approx 4T$, while the difference curve peaks at $E \approx 3.3T$. All curves have exponential tails that become small for $E \gtrsim 13T$.

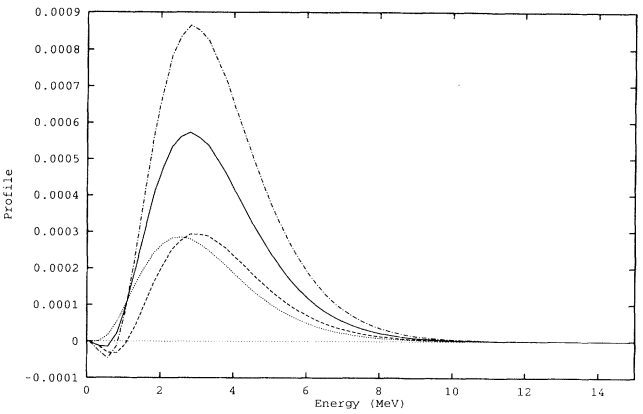

FIG. 1. Pure-production profiles. For zero mixing angle and at $T = 0.75$ MeV, the excess-neutrino number per unit energy in the canonical comoving volume is shown as a function of energy. The solid line is electron neutrinos, the dashed line is muon neutrinos, the dotted line is their difference, and the dashed-dotted line is their sum.

The distortion curves in Fig. 1 evolve with time for $t > t_f$ due to the expansion of the Universe and the associated energy redshifts. For $T < 0.75$ MeV, the curves maintain the same overall shape but are compressed horizontally and expanded vertically by the factor T_f/T, where $T_f = 0.75$ MeV. Thus, at later times the peaks at ~ 3.0 MeV approach the origin and increase in height. The areas under the curves remain constant, since neutrinos are neither created nor destroyed when $t > t_f$.

It is useful to have analytical expressions representing the pure-production profiles in Fig. 1. We find the electron- and muon-neutrino profile curves are accurately reproduced by the expressions

$$\begin{aligned}\nu_e^\dagger\nu_e(E)/T \approx (&-1.3567\times10^{-2}+1.9692\times10^{-2}x+2.4600\times10^{-3}x^2\\&+5.9818\times10^{-5}x^3-7.5683\times10^{-6}x^4)\frac{x^2}{2\pi^2}\exp(-x)\ ,\\ \nu_\mu^\dagger\nu_\mu(E)/T \approx (&-1.0568\times10^{-2}+1.0668\times10^{-2}x+1.4263\times10^{-3}x^2\\&+9.1969\times10^{-5}x^3-7.5711\times10^{-6}x^4)\frac{x^2}{2\pi^2}\exp(-x)\ ,\end{aligned} \tag{7.1}$$

where $x = E/T$.

Figure 2 presents a comparison of our electron-neutrino and neutrino-difference profiles with the estimate of Ref. [16], which is

$$\nu_e^\dagger\nu_e(E)/T = (6\times10^{-4})\frac{E}{T}\left(\frac{11E}{4T}-3\right)\times\frac{E^2}{2\pi^2}e^{-E/T}a^3\ . \tag{7.2}$$

Our results exhibit two principal differences from those of Ref. [16]. First, the analytical approximation (7.2) somewhat overestimates the electron-neutrino excess. In the canonical volume a^3 with $a(t) = 2.0$ MeV^{-1} at $t = t_f$, we obtain a total electron-neutrino excess of about 2×10^{-3}. In contrast, the analytical approximation (7.2) gives about 4.8×10^{-3}. Second, our distortions reach a maximum at a slightly lower energy. The peak in our neutrino-difference profile occurs at an energy value about 25% below that of the peak in Eq. (7.2).

The total muon-neutrino excess we obtain in the canonical volume is about 1×10^{-3} so that the total excess of electron neutrinos over muon neutrinos is also about

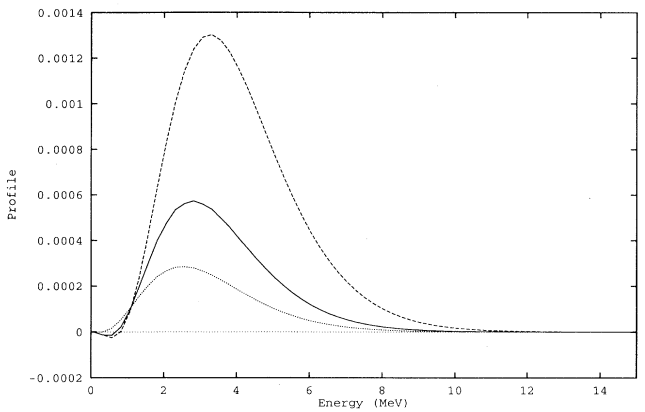

FIG. 2. Comparison of pure-production profiles. For zero mixing angle and at $T = 0.75$ MeV, the excess-neutrino number per unit energy in the canonical comoving volume is shown as a function of energy. The solid line is our electron-neutrino results, the dotted line is the difference between our electron- and muon-neutrino results, and the dashed line is the analytical approximation of Ref. [16].

1×10^{-3}. Since the oscillation simulations in Refs. [11–13] were based on the initial production profile (7.2), our current simulations lead to some modifications of the earlier results. These effects are discussed in Sec. IX.

Figure 3 shows the time development of the nonequilibrium distortions. Various combinations of components of the average neutrino vector are plotted as functions of time. The curves begin at $t_s \approx 0.082$ s and end at the final production time of $t_f \approx 1.312$ s. The production proceeds smoothly and monotonically. The total number of excess electron neutrinos in the canonical volume corresponds to $\langle(v_0 + v_1)/2\rangle$, while the total number of excess muon neutrinos corresponds to $\langle(v_0 - v_1)/2\rangle$. The difference between electron and muon neutrinos is given by the component $\langle v_1\rangle$, while their sum is $\langle v_0\rangle$. The total excess of τ neutrinos is the same as for μ neutrinos, and hence is given by $\langle v_4\rangle = \langle(v_0 - v_1)/2\rangle$. Again, CP symmetry ensures that the results for antineutrinos are the same as those for neutrinos.

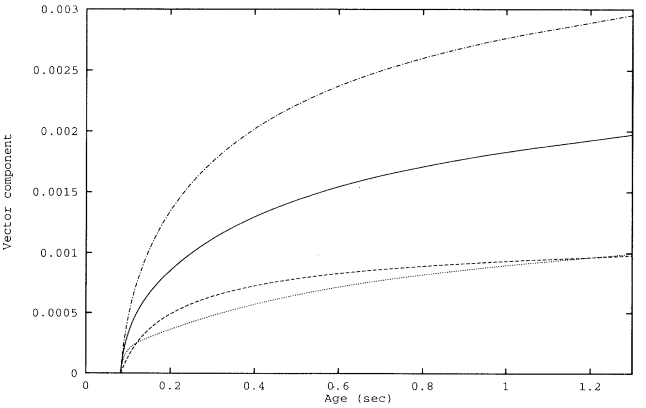

FIG. 3. Time development of nonequilibrium distortions. The solid line is the total excess of electron neutrinos in the canonical comoving volume as a function of time. The dashed line is the total muon-neutrino excess, the dotted line is the difference between electron and muon neutrinos, and the dashed-dotted line is their sum.

Overall, our results for pure production are similar to those of Ref. [15]. The final neutrino distortion productions in Ref. [15] were terminated at 0.1 MeV. When extrapolated to T_f, they are about 35% larger than ours but are otherwise comparable. As previously noted, the difference lies in the treatment of the electron mass. However, since we do not assume neutrinos are in thermal equilibrium at very early times, our early-time results differ. For instance, taking into account thermalizing neutrino interactions, we find that the $T = 8$ MeV electron-neutrino distortion Δ_{ν_e} is virtually zero, unlike the results in Fig. 4 of Ref. [15]. For the same reason, we find a much smaller profile at $T = 4$ MeV. Similarly, our results for Figs. 5–8 of Ref. [15] produce curves dropping sharply for $T \gtrsim 4$ MeV, without the $1/T^2$ behavior for early times.

VIII. RESULTS FOR PRODUCTION WITH OSCILLATIONS

This section discusses our numerical results for the production of nonequilibrium distributions when neutrino mixing is present.

For $\Delta < 10^{-8}$ eV^2, our results resemble the $\theta = 0$ case discussed in Sec. VII. This follows because the vacuum term is small for $t_s < t < t_f$ and $\Delta < 10^{-8}$ eV^2. The neutrino vectors, antineutrino vectors, and effective magnetic fields are all directed near the flavor axis, i.e., the one-axis. Since they point in a common direction, the cross-product terms $\vec{v} \times \vec{B}_v$ and $\vec{w} \times \vec{B}_w$ in Eqs. (5.8) and (5.9) are close to zero, and production proceeds as if there were no neutrino mixing.

When $\Delta > 10^{-8}$ eV^2, some excess electron neutrinos convert to muon neutrinos during the production phase. As expected, the effect is greater for larger θ. As a consequence of the neutrino conversion, the electron-neutrino and difference profiles are reduced while the muon-neutrino profile is increased.

Figure 4 displays the results for $\Delta = 10^{-6}$ eV^2 and $\sin^2 2\theta = 0.81$. The curves representing the e- and μ-neutrino sum profile and the τ-neutrino profile are almost identical to those in Fig. 1. This also holds true at other values of Δ and θ. The reason is that the oscillation terms do not directly enter the expressions for these profiles, as can be seen from Eqs. (5.8) and (5.9). Thus, oscillations affect them only by feedback from the conversion among electron and muon neutrinos into the scattering processes in the Boltzmann equation. This secondary effect is relatively small.

We have constructed an analytical approximation to the production profiles when $0 < \theta < \pi/4$, given the pure-production results. It is based on the following idea. In a small time interval during production, a new excess of electron neutrinos is supplied to the system. This corresponds to adding small components to neu-

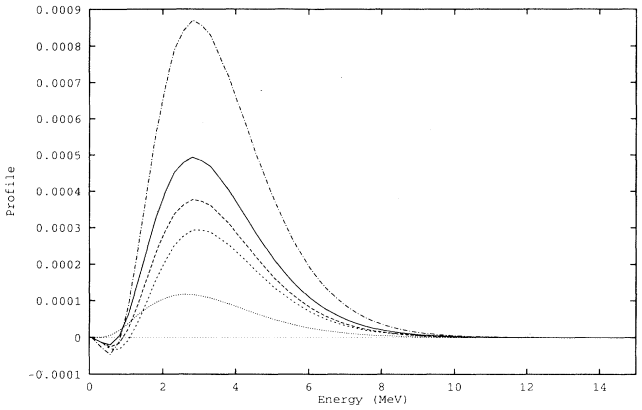

FIG. 4. Production profiles for $\Delta = 10^{-6}$ eV^2 and $\sin^2 2\theta = 0.81$. The excess-neutrino number per unit energy in the canonical comoving volume is shown as a function of energy. The solid line is electron neutrinos, the dashed line is muon neutrinos, the dotted line is their difference, the dashed-dotted line is their sum, and the short-dashed line is tau neutrinos.

trino vectors along the one-axis. These small additional components rotate around the associated magnetic fields. Since the production is continuous and since the time scale for oscillations is much shorter than the time scale for production, when averaged over an oscillation time the new small components lead to contributions aligned with the magnetic fields. Thus, ANME configurations are achieved. The averaging effect is equivalent to projecting the production vectors onto their magnetic fields. To construct analytical ANME configurations, we exploit the scheme presented in Ref. [13] and mentioned in Sec. IV: the partial cancellation between the neutrino-neutrino and CP-asymmetric terms means that reasonably accurate ANME configurations can be obtained using only the vacuum and CP-symmetric terms. Then, for each E one projects the new production contributions onto the analytical ANME configurations. This must be done continuously during the production phase, and the results summed.

It is useful to find a simpler approach based on the final pure-production profile. Then, one can employ the fits in Eq. (7.2). In much of the parameter region of our simulations, the magnetic fields governing neutrino oscillations are changing. Initially, the magnetic fields point along the one-axis. Hence, ANME configurations are flavor eigenstates. For $\Delta > 10^{-8}$ V^2, magnetic fields rotate toward $\vec{\Delta}$ during the later stages of production. If most of the production occurs before this rotation, then the production profile for $\theta \neq 0$ is obtained by *rotating* the pure-production case, for which $\theta = 0$, onto ANME configurations. If most of the production occurs after the rotation, then the production profile for $\theta \neq 0$ is obtained by *projecting* the pure-production case onto ANME configurations. In general, early production is rotated onto ANME configurations, while later production is projected. Hence, we expect the true production profile to lie between the projected and rotated curves.

The analytical approximation to the data is implemented as follows. It is understood that all vectors in this paragraph have three components. Define the CP-symmetric part $\vec{B}_+$ of the magnetic field by

$$\vec{B}_+(E,t) = \frac{\vec{\Delta}}{2E} - V_{CP+}(E)\hat{e}_1 \ . \tag{8.1}$$

Let $\vec{v}^{(0)}(E,t_f)$ be the vector obtained in numerical simulations for pure production with $\theta = 0$. Then, the rotated vector $\vec{v}_r(E,t_f)$ is given by

$$\vec{v}_r(E,t_f) = \pm\frac{|\vec{v}^{(0)}(E,t_f)|}{|\vec{B}_+(E,t_f)|}\vec{B}_+(E,t_f) \ , \tag{8.2}$$

where the $\pm$ sign is the sign of $\vec{v}^{(0)}(E,t_f)\cdot\vec{B}_+(E,t_f)$. The projected vector $\vec{v}_p(E,t_f)$ is given by

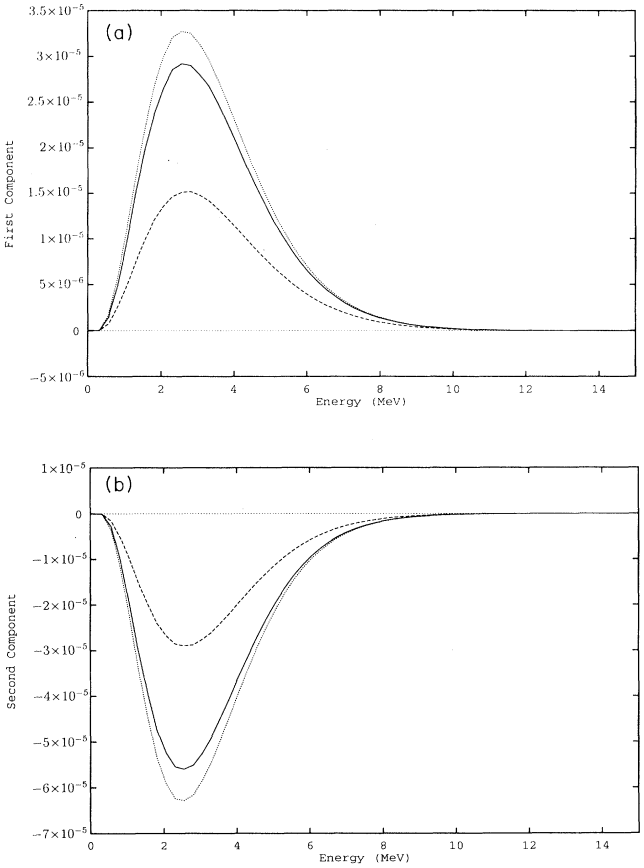

FIG. 5. Analytical approximations to profile plots for $\Delta = 10^{-6}$ eV^2, $\sin^2 2\theta = 0.81$. The solid lines are the data, the dashed lines are the projection approximation (8.3), and the dotted lines are the rotation approximation (8.2). (a) The first component of the neutrino vector as a function of energy. (b) The second component of the neutrino vector as a function of energy.

$$\vec{v}_p(E,t_f) = \frac{\vec{v}^{(0)}\cdot\vec{B}_+(E,t_f)}{\vec{B}_+\cdot\vec{B}_+(E,t_f)}\vec{B}_+(E,t_f)\ . \qquad (8.3)$$

The analytical approximation based on rotation, with data approximated using Eq. (8.2), works quite well for small Δ or small θ. For example, when $\Delta < 10^{-7}$ eV^2, the agreement for $v_1(E,t_f)$ and $v_2(E,t_f)$ is at the 1% level even for the large-angle case with $\sin^2 2\theta = 0.81$. The same accuracy is obtained for the case with $\Delta = 10^{-6}$ eV^2 with $\sin^2 2\theta = 0.25$.

Figures 5(a) and 5(b) show profile plots of the components v_1 and v_2 for the case $\Delta = 10^{-6}$ eV^2, $\sin^2 2\theta = 0.81$. As expected, the data lie between the two analytical approximations based on rotation and on projection. In the region where E is a few MeV, the analytical rotation method overestimates the vectors by about 10%. The error reduces to about 5% in the energy range near 8 MeV, while for $E \gtrsim 11$ MeV the method is accurate to at least one percent. The higher-energy vectors are reproduced better because their magnetic fields undergo relatively less rotation.

The analytical approximation also works at earlier times during the production process. The idea is to use Eq. (8.2) or (8.3) with the final time t_f replaced by an arbitrary time t in the production interval $t_s < t \leq t_f$. For example, consider the time $t \approx 0.5$ s in the middle region of the production phase for the case with $\Delta = 10^{-4}$ eV^2 and $\sin^2 2\theta = 0.81$. As expected, our data show that the values of v_1 and v_2 again fall between the curves obtained from the rotation and projection approximations. For $E > 4$ MeV, the rotation method fits the data to about 10%. For $E < 4$ MeV, the rotation results are larger than the data, with significant deviations when $E < 2$ MeV. For $E < 2$ MeV, the projection method underestimates the data by about 30%. The projection approximation is better for low-energy neutrinos here because the corresponding ANME configurations undergo significant early rotation during production.

In the parameter region with $\Delta > 10^{-4}$ eV^2, the full simulation of the production phase involves prohibitive computer time. The production profile should lie closer to the projection method based on Eq. (8.3). For $\Delta > 10^{-2}$ eV^2, the projection approximation should be reasonably accurate. Indeed, in a test run for $\sin^2 2\theta = 0.81$ and $\Delta = 10^{-1}$ eV^2, the data were reproduced within statistical uncertainties.

The analytical approximation and the insights obtained in our earlier work, summarized in Sec. IV, suggest several predictions for neutrino behavior during the production phase. First, neutrinos should maintain themselves in ANME configurations. Second, the flavor development of neutrinos should be smooth. This follows from the ANME property and the slow evolution of the effective magnetic fields during the production time interval from t_s to t_f. Third, alignment should hold. This is a consequence of the ANME property and the approximate alignment of the effective magnetic fields. Fourth, there should be planarity. This follows because instantaneous nonlinear mass eigenstates have $v_3 = 0$ and so, since the neutrinos are in ANME configurations, v_3 should be much smaller than v_1 and v_2. Finally, CP asymmetry should be suppressed. The ANME property implies the existence of the mechanism for CP-asymmetry cancellation given in Ref. [13].

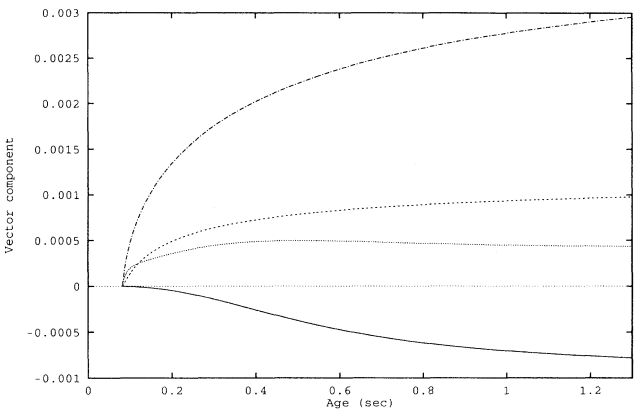

FIG. 6. Components of the average neutrino vector as a function of time for the case with $\Delta = 10^{-6}$ eV^2 and $\sin^2 2\theta = 0.81$. The dashed-dotted line is the zeroth component, the dotted line is the first component, the solid line is the second component, and the short-dashed line is the fourth component. The third component is indistinguishable from zero on the scale of the figure.

Data obtained during our production runs confirm these five predictions. All the data display smooth neutrino-flavor behavior. Figure 6 shows the components of the average neutrino vector as a function of time for the case with $\Delta = 10^{-6}$ eV^2 and $\sin^2 2\theta = 0.81$. The smooth behavior is evident. The planarity feature is also evident since the third component is small. In fact, the third component is at least three orders of magnitude smaller than the first component. The antineutrino-vector components are omitted from Fig. 6 because they are indistinguishable from the vector components on the scale of the figure. The difference between neutrino and antineutrino vectors is typically four or more orders of magnitude smaller than the vectors themselves. This reflects the CP-suppression mechanism. We also examined data taken during the $\Delta = 10^{-4}$ eV^2 and $\sin^2 2\theta = 0.81$ production cycle, which is expected to exhibit the most sensitive dependence on the ANME and alignment properties. The data reveal that these properties hold well. The test results are similar to those shown in Table IV of Ref. [13].

IX. RESULTS FOR PURE OSCILLATIONS AFTER PRODUCTION

This section describes results for oscillations governed by Eq. (3.2) but based on the final production profile obtained from the Boltzmann equation with oscillations. We also discuss some differences with results in our earlier works [11–13], in which the production profile is treated in a step-function approximation based on the analytical approximation of Ref. [16] given by Eq. (7.2). For pur-

poses of comparison with the earlier work, we introduce in this section the normalized vectors $\vec{r}_\nu(t)$ defined by

$$\vec{r}_\nu(t) = \frac{\langle \vec{v}(t) \rangle}{\langle |\vec{v}(t)| \rangle} . \tag{9.1}$$

In this equation, $\langle |\vec{v}(t)| \rangle = \sum_j |\vec{v}^j(t)|$ is the total number of neutrinos in the canonical comoving volume at time t, which is constant during the oscillation phase $t > t_f$ because neutrinos are neither created nor destroyed in the comoving volume.

Figure 7 displays the components $r_{\nu 1}$ and $r_{\nu 2}$ as a function of time for the case with $\Delta = 10^{-12}$ eV^2 and $\sin^2 2\theta = 0.81$. The solid lines represent our new data, while the dashed lines represent data from earlier work [13]. The figure shows that a flavor conversion occurs about 5 s earlier in our new data.

The qualitative features of the two sets of data agree. In both sets of data, the behavior is evolutionary and smooth. At early times with $t < 40$ s, neutrinos are in approximate flavor eigenstates and hence the neutrino vectors lie along the one-axis. The relatively small initial vacuum term grows with time and eventually dominates, so that for $t > 120$ s the neutrinos are instead in approximate vacuum-mass eigenstates with their vectors lying along $\vec{\Delta}$. Both sets of data display a feature called precocious rotation; i.e., the rotation to vacuum-mass eigenstates occurs significantly earlier than in the absence of the nonlinear term. The results differ significantly from data taken in the absence of neutrino-neutrino interactions. Without the nonlinear term, magnetic fields are dominated by the vacuum term only for $t \gtrsim 500$ s, damped oscillations occur, and neutrinos attain vacuum behavior only after $t > 1500$ s.

The reason for the earlier flavor conversion in the new data is the use of our new production profile. As noted in the discussion below Eq. (7.2), there are two main differences between our new profile and the one obtained in Ref. [16]: the total production is smaller, and the average energy is lower. See Fig. 2. The change in the total production largely cancels in the ratio $\vec{r}_\nu$. It is the energy shift that is responsible for the 5-s time difference appearing in Fig. 7. The partial cancellation between the terms $\vec{V}_{\nu\nu}$ and V_{CP-} means that the precocious rotation occurs when $|\vec{\Delta}/2E|$ and $|V_{CP+}(E)|$ become approximately equal [13]. When the average energy of the profile is smaller, the vacuum term is larger and so the rotation to vacuum-mass eigenstates occurs sooner.

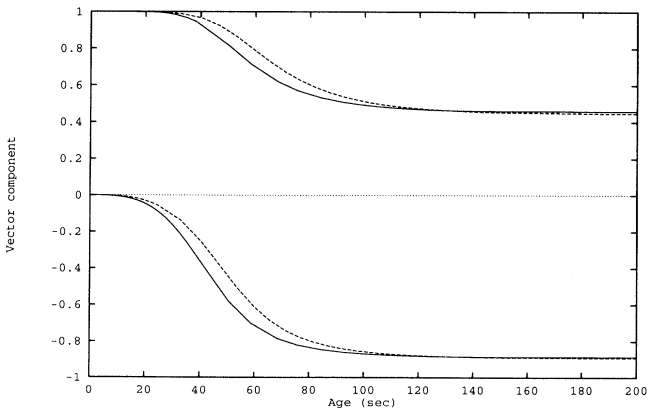

FIG. 7. Components of the normalized average neutrino vector $\vec{r}_\nu(t)$ as a function of time for the case with $\Delta = 10^{-12}$ eV^2 and $\sin^2 2\theta = 0.81$. The solid lines represent the new data, while the dashed lines represent data from earlier work [13]. The curves above the horizontal axis are the component $r_{\nu 1}$, while the curves below it are the component $r_{\nu 2}$.

A similar effect appears for other values of Δ and $\sin^2 2\theta$. For example, the curves for $r_{\nu 1}$ and $r_{\nu 2}$ in the case with $\Delta = 10^{-9}$ eV^2 and $\sin^2 2\theta = 0.81$ are shifted relative to our earlier results by about 1 s in the crossover region between 3 and 16 s. This is again due to the smaller average energy of the profile, which causes an early rotation to vacuum-mass eigenstates because ANME configurations align sooner with $\vec{\Delta}$. Beyond 16 s, the two sets of data coincide. Likewise, the curves for $r_{\nu 1}$ and $r_{\nu 2}$ in the case with $\Delta = 10^{-6}$ eV^2 and $\sin^2 2\theta = 0.81$ display time shifts of about 0.1 s in the crossover region between 0.3 and 1.5. Beyond 2.0 s, results again coincide. For cases with smaller mixing angles, the time-difference effect is comparable but is less pronounced in plots because the neutrino flavor changes less. We remark in passing that the effect is absent for the case with $\Delta = 10^{-4}$ eV^2 and $\sin^2 2\theta = 0.81$ because the overlap between the new data and those of Ref. [13] occurs when neutrinos are already near vacuum-mass eigenstates.

The results we have obtained confirm all the qualitative conclusions of Ref. [13], summarized in Sec. IV. The numerical results of [13] are accurate, except for the above-mentioned time-shift effect in the crossover region.

The analytical approximations obtained in the present work and in Ref. [13] provide a means to determine neutrino vectors to an accuracy better than the intrinsic methodological uncertainties discussed in Sec. II. There are two stages involved. First, given a value of Δ and $\sin^2 2\theta$, the neutrino-distortion production profile can be determined via the techniques provided in Sec. VIII. Second, results for post-production times $t > t_f$ can be found using the method of Sec. VI E in Ref. [13]. This method gives the neutrino vectors as

$$\vec{v}(E,t) \approx \pm \frac{|\vec{v}(E,t_f)|}{|\vec{B}_+(E,t)|} \vec{B}_+(E,t) , \tag{9.2}$$

where $\vec{B}_+(E,t)$ is defined in Eq. (8.1), and where the overall sign is that of the dot product $\vec{v}(E,t_f)\cdot\vec{B}_+(E,t_f)$. The antineutrino vectors are set equal to the neutrino vectors, $\vec{w}(E,t) = \vec{v}(E,t)$, thus guaranteeing perfect CP suppression. The third components of vectors are zero, thus ensuring planarity. The second stage of the method reproduces numerical results to about two decimal places [13]. Via this two-step procedure, reasonably accurate numbers for all quantities can be obtained.

X. SUMMARY

In this work, we have treated the nonequilibrium thermodynamic statistics of neutrinos in the early Universe

in the presence of neutrino mixing and oscillations. Differential equations were derived that determine the deviations from standard equilibrium statistics. They are Eqs. (5.8) and (5.9). We have resorted to numerical methods to solve these equations, since they are complicated and nonlinear. We summarize here the behavior of the solutions and our methods for approximating them analytically.

Soon after the start of the production of nonequilibrium distortions, neutrinos and antineutrinos achieve configurations that are approximate nonlinear mass eigenstates (ANME). As the Universe expands, various interaction terms change. However, the neutrinos remain in ANME configurations during these changes, so the flavor content evolves smoothly.

For $\Delta < 10^{-8}$ eV^2, the production of nonequilibrium distortions occurs when the vacuum term is relatively small. This implies that the production phase proceeds as in the case without neutrino mixing, producing neutrinos close to flavor eigenstates. During the oscillation phase, the vacuum term increases while the interaction effects decrease. Eventually, the vacuum term dominates. Neutrinos therefore gradually evolve from flavor eigenstates to vacuum-mass eigenstates. For $\Delta < 10^{-9}$ eV^2, the rotation occurs earlier than one might expect if neutrino-neutrino interactions are neglected. This precocious rotation, observed and explained in Ref. [13], is confirmed in our simulations.

For $\Delta > 10^{-8}$ eV^2, oscillations play a significant role already during the production phase. Since the nonequilibrium distortions are induced by the weak interactions, the excess neutrinos are generated as flavor eigenstates. However, the time scale for oscillations is much shorter than that for production, so the neutrinos quickly oscillate, decohere, and achieve ANME configurations. For $\Delta < 10^{-7}$ eV^2 much of the production occurs while ANME configurations point in the flavor direction. Hence, a good approximation to the final production profile in this case is to *rotate* the final pure-production (zero mixing) results onto ANME configurations. For $\Delta > 10^{-2}$ eV^2 most of the production occurs while ANME configurations point in the mass-eigenstate direction. Hence, a good approximation to the final production profile in this case is to *project* the pure-production results onto ANME configurations. In the region 10^{-7} eV$^2 < \Delta < 10^{-2}$ eV^2, these two approximations straddle the true production results.

The above approximations to the final production profile can be made analytical by using the cancellation mechanism of Ref. [13] so that mass eigenstates are constructed based solely on the vacuum term and the CP-conserving interaction between the charged leptons and the neutrinos. For the parameter region of our simulations, we find that the rotation method reproduces the data extremely well for $\Delta < 10^{-7}$ eV^2. For $\Delta \approx 10^{-6}$ eV^2 and $\sin^2 2\theta = 0.81$, it overestimates results by at most 10%. One can compensate for this effect. We have also described in Sec. VIII how to extend the analytical method to the production-oscillation results for larger Δ.

During the oscillation phase for $\Delta > 10^{-8}$ eV^2, neutrinos continue to rotate toward vacuum-mass eigenstates. The behavior therefore continues to be smooth and evolutionary. For $\Delta > 10^{-2}$ eV^2, we expect the production phase to render neutrinos close to vacuum-mass eigenstates. Since the vacuum term dominates thereafter, neutrinos remain in vacuum-mass eigenstates during the oscillation phase. The result should be constant flavor behavior. Indeed, short test simulations confirm this.

The improved treatment of the production phase means that our results for *unnormalized* quantities are now accurate to within systematic uncertainties. This represents an improvement in absolute accuracy of a factor of about twenty.

The approximate analytical method of Ref. [13] can be used to obtain to good precision the results for the oscillation phase. By combining this method with the new analytical treatment of the production, we obtain a complete analytical approximation for the neutrino and antineutrino vectors over the entire time period of interest.

All the qualitative neutrino flavor behavior of Refs. [11,13] has been confirmed. Features including smooth evolutionary behavior, alignment, planarity, maintenance of ANME configurations, and CP suppression are observed not only in the oscillation phase but also during the production phase.

We have uncovered one quantitative difference with Ref. [13]: neutrinos rotate to vacuum-mass eigenstates about 5% earlier in time. The reason is that the approximate initial distortion distributions used in Ref. [13] are shifted somewhat to higher energies than those produced in our present numerical data. This caused the vacuum term to dominate somewhat later in the simulations of Ref. [13]. Asymptotically, the results of our current and previous work agree.

Within the parameter region of this paper, we have found little generation of CP asymmetry. This means that nonequilibrium distortions are unlikely to affect nucleosynthesis substantially. Although one might *a priori* expect neutrino oscillations to have observable effects, the CP-suppression mechanism we uncovered in our simulations implies that the impact on the primordial helium abundance is likely to be at the same level as found in Ref. [15], where neutrino mixing was absent.

ACKNOWLEDGMENTS

We thank Scott Dodelson and Mike Turner for discussions and for making available to us their pure-production data. This work was supported in part by the United States Department of Energy (Grant Nos. DE-FG02-91ER40661 and DE-FG02-92ER40698) by the Alexander von Humboldt Foundation, and by the PSC Board of Higher Education at CUNY.

APPENDIX A: COEFFICIENTS FOR THREE-FLAVOR PURE PRODUCTION

This appendix provides the A, B, and C coefficients appearing in Eq. (2.7). They are functions of the scaled

initial and final neutrino energies $\frac{E}{T}$ and $\frac{E'}{T}$. This functional dependence is dropped here to save space. In what follows, it is useful to define the electroweak coupling constants

$$a \equiv (1+\sin^2\theta_w)^2, \quad b \equiv (2\sin^2\theta_w)^2, \quad c \equiv (1-\sin^2\theta_w)^2, \tag{A1}$$

where the squared weak-mixing angle is

$$\sin^2\theta_w \approx 0.2325 . \tag{A2}$$

The A coefficients are given by

$$A_{\bar{\nu}_e} = A_{\nu_e} \equiv \left(\frac{5(a+b)+17}{3}\right)\frac{E}{T} , \tag{A3}$$

$$A_{\bar{\nu}_\tau} = A_{\nu_\tau} = A_{\bar{\nu}_\mu} = A_{\nu_\mu} \equiv \left(\frac{5(b+c)+17}{3}\right)\frac{E}{T} .$$

The B coefficients are

$$B_{\bar{\nu}_e} = B_{\nu_e} \equiv (a+b)\frac{E}{T}\left(\frac{11}{12}\frac{E}{T}-1\right)\exp\left(-\frac{E}{T}\right) , \tag{A4}$$

$$B_{\bar{\nu}_\tau} = B_{\nu_\tau} = B_{\bar{\nu}_\mu} = B_{\nu_\mu} \equiv (b+c)\frac{E}{T}\left(\frac{11}{12}\frac{E}{T}-1\right)\exp\left(-\frac{E}{T}\right) .$$

The C coefficients are expressed in terms of functions $\bar{g}_i$, presented in Eq. (A12) below. For the electron neutrino, we find

$$\begin{aligned}
&C_{\nu_e\nu_e} = C_e^1\bar{g}_1 + C_e^2\bar{g}_3 + 2C_e^1\bar{g}_2 + 3\bar{g}_0 ,\\
&C_{\nu_e\nu_\mu} = \bar{g}_1 + 2\bar{g}_3 + 2\bar{g}_2 + 3\bar{g}_0 ,\\
&C_{\nu_e\nu_\tau} = \bar{g}_1 + 2\bar{g}_3 + 2\bar{g}_2 + 3\bar{g}_0 ,\\
&C_{\nu_e\bar{\nu}_e} = 4\bar{g}_1 + C_e^1\bar{g}_0, \quad C_{\nu_e\bar{\nu}_\mu} = 2\bar{g}_1 + \bar{g}_0 ,\\
&C_{\nu_e\bar{\nu}_\tau} = 2\bar{g}_1 + \bar{g}_0 .
\end{aligned} \tag{A5}$$

For the muon neutrino, we find

$$\begin{aligned}
&C_{\nu_\mu\nu_\mu} = C_\mu^1\bar{g}_1 + C_\mu^2\bar{g}_3 + 2C_\mu^1\bar{g}_2 + 3\bar{g}_0 ,\\
&C_{\nu_\mu\nu_e} = \bar{g}_1 + 2\bar{g}_3 + 2\bar{g}_2 + 3\bar{g}_0 ,\\
&C_{\nu_\mu\nu_\tau} = \bar{g}_1 + 2\bar{g}_3 + 2\bar{g}_2 + 3\bar{g}_0 ,\\
&C_{\nu_\mu\bar{\nu}_e} = 2\bar{g}_1 + \bar{g}_0, \quad C_{\nu_\mu\bar{\nu}_\mu} = 4\bar{g}_1 + C_\mu^1\bar{g}_0 ,\\
&C_{\nu_\mu\bar{\nu}_\tau} = 2\bar{g}_1 + \bar{g}_0 .
\end{aligned} \tag{A6}$$

For the tau neutrino, we find

$$\begin{aligned}
&C_{\nu_\tau\nu_\tau} = C_\mu^1\bar{g}_1 + C_\mu^2\bar{g}_3 + 2C_\mu^1\bar{g}_2 + 3\bar{g}_0 ,\\
&C_{\nu_\tau\nu_e} = \bar{g}_1 + 2\bar{g}_3 + 2\bar{g}_2 + 3\bar{g}_0 ,\\
&C_{\nu_\tau\nu_\mu} = \bar{g}_1 + 2\bar{g}_3 + 2\bar{g}_2 + 3\bar{g}_0 ,\\
&C_{\nu_\tau\bar{\nu}_e} = 2\bar{g}_1 + \bar{g}_0, \quad C_{\nu_\tau\bar{\nu}_\mu} = 2\bar{g}_1 + \bar{g}_0 ,\\
&C_{\nu_\tau\bar{\nu}_\tau} = 4\bar{g}_1 + C_\mu^1\bar{g}_0 .
\end{aligned} \tag{A7}$$

For the electron antineutrino, we find

$$\begin{aligned}
&C_{\bar{\nu}_e\nu_e} = 4\bar{g}_1 + C_e^1\bar{g}_0, \quad C_{\bar{\nu}_e\nu_\mu} = 2\bar{g}_1 + \bar{g}_0 ,\\
&C_{\bar{\nu}_e\nu_\tau} = 2\bar{g}_1 + \bar{g}_0 ,\\
&C_{\bar{\nu}_e\bar{\nu}_e} = C_e^1\bar{g}_1 + C_e^2\bar{g}_3 + 2C_e^1\bar{g}_2 + 3\bar{g}_0 ,\\
&C_{\bar{\nu}_e\bar{\nu}_\mu} = \bar{g}_1 + 2\bar{g}_3 + 2\bar{g}_2 + 3\bar{g}_0 ,\\
&C_{\bar{\nu}_e\bar{\nu}_\tau} = \bar{g}_1 + 2\bar{g}_3 + 2\bar{g}_2 + 3\bar{g}_0 .
\end{aligned} \tag{A8}$$

For the muon antineutrino, we find

$$\begin{aligned}
&C_{\bar{\nu}_\mu\nu_e} = 2\bar{g}_1 + \bar{g}_0, \quad C_{\bar{\nu}_\mu\nu_\mu} = 4\bar{g}_1 + C_\mu^1\bar{g}_0 ,\\
&C_{\bar{\nu}_\mu\nu_\tau} = 2\bar{g}_1 + \bar{g}_0 ,\\
&C_{\bar{\nu}_\mu\bar{\nu}_\mu} = C_\mu^1\bar{g}_1 + C_\mu^2\bar{g}_3 + 2C_\mu^1\bar{g}_2 + 3\bar{g}_0 ,\\
&C_{\bar{\nu}_\mu\bar{\nu}_e} = \bar{g}_1 + 2\bar{g}_3 + 2\bar{g}_2 + 3\bar{g}_0 ,\\
&C_{\bar{\nu}_\mu\bar{\nu}_\tau} = \bar{g}_1 + 2\bar{g}_3 + 2\bar{g}_2 + 3\bar{g}_0 .
\end{aligned} \tag{A9}$$

For the tau antineutrino, we find

$$\begin{aligned}
&C_{\bar{\nu}_\tau\nu_e} = 2\bar{g}_1 + \bar{g}_0, \quad C_{\bar{\nu}_\tau\nu_\mu} 2\bar{g}_1 + \bar{g}_0 ,\\
&C_{\bar{\nu}_\tau\nu_\tau} = 4\bar{g}_1 + C_\mu^1\bar{g}_0 ,\\
&C_{\bar{\nu}_\tau\bar{\nu}_\tau} = C_\mu^1\bar{g}_1 + C_\mu^2\bar{g}_3 + 2C_\mu^1\bar{g}_2 + 3\bar{g}_0 ,\\
&C_{\bar{\nu}_\tau\bar{\nu}_e} = \bar{g}_1 + 2\bar{g}_3 + 2\bar{g}_2 + 3\bar{g}_0 ,\\
&C_{\bar{\nu}_\tau\bar{\nu}_\mu} = \bar{g}_1 + 2\bar{g}_3 + 2\bar{g}_2 + 3\bar{g}_0 .
\end{aligned} \tag{A10}$$

In Eqs. (A5)–(A10), we use the abbreviations

$$\begin{aligned}
&C_e^1 \equiv a+b+6, \quad C_\mu^1 \equiv b+c+6 ,\\
&C_e^2 \equiv 2(a+b)+10, \quad C_\mu^2 \equiv 2(b+c)+10 .
\end{aligned} \tag{A11}$$

The $\bar{g}$ are scaled versions of the functions g of Ref. [15]:

$$\begin{aligned}
\bar{g}_0\left(\frac{E}{T},\frac{E'}{T}\right) &\equiv -\frac{1}{18}\frac{E}{T}\left(\frac{E'}{T}\right)^3\exp\left(-\frac{E}{T}\right) ,\\
\bar{g}_1\left(\frac{E}{T},\frac{E'}{T}\right) &\equiv \frac{1}{64}\exp\left(\frac{E'-E}{2T}\right)\left(\frac{T}{E}\right)^2 g_1\left(\frac{E}{T},\frac{E'}{T}\right) ,\\
\bar{g}_2\left(\frac{E}{T},\frac{E'}{T}\right) &\equiv \frac{1}{64}\exp\left(\frac{E'-E}{2T}\right)\left(\frac{T}{E}\right)^2 g_2\left(\frac{E}{T},\frac{E'}{T}\right) ,\\
\bar{g}_3\left(\frac{E}{T},\frac{E'}{T}\right) &\equiv \frac{1}{64}\exp\left(\frac{E'-E}{2T}\right)\left(\frac{T}{E}\right)^2 g_3\left(\frac{E}{T},\frac{E'}{T}\right) .
\end{aligned} \tag{A12}$$

For completeness we give the unbarred $g_i\left(\frac{E}{T},\frac{E'}{T}\right)$:

$$\begin{aligned}
g_1\left(\frac{E}{T},\frac{E'}{T}\right) &= \int_{|v|}^{w} dy e^{-\frac{y}{2}}(v^2-y^2)^2 ,\\
g_2\left(\frac{E}{T},\frac{E'}{T}\right) &= -\int_{|v|}^{w}\frac{dy}{2y^2}e^{-\frac{y}{2}}(v^2-y^2)^2(2w+wy+y^2) ,\\
g_3\left(\frac{E}{T},\frac{E'}{T}\right) &= \int_{|v|}^{w}\frac{dy}{4y^4}e^{-\frac{y}{2}}(v^2-y^2)^2\\
&\quad\times[12w^2+6w^2y+(w^2+4w-4)y^2\\
&\quad+2(w-1)y^3+y^4] ,
\end{aligned} \tag{A13}$$

where the abbreviations

$$v \equiv \frac{(E-E')}{T}, \quad w \equiv \frac{(E+E')}{T}, \quad x \equiv \frac{E}{T} \tag{A14}$$

are used. The lower limit of each integration in Eq. (A13) is the absolute value of v. Note that the above expression for g_3 differs from that in Ref. [15], which is incorrectly typeset.

APPENDIX B: COEFFICIENTS FOR COMBINED PRODUCTION-OSCILLATION

Here, we express the coefficients A_{ab}, $A_{\bar{a}\bar{b}}$, B_a, $B_{\bar{a}}$, C_{ab}, $C_{a\bar{b}}$, $C_{\bar{a}b}$, and $C_{\bar{a}\bar{b}}$ in the vector basis in terms of the coefficients A_{ν_f}, $\tilde{B}_{\nu_f}$, and $\tilde{C}_{\nu_f\nu_{f'}}$. Since all coefficients are functions of the scaled initial and final neutrino energies $\frac{E}{T}$ and $\frac{E'}{T}$, we drop this dependence everywhere to save space.

The nonzero A_{ab} and $A_{\bar{a}\bar{b}}$ are

$$\begin{aligned} A_{00} &= A_{11} = \frac{1}{2}(A_{\nu_e} + A_{\nu_\mu}), \\ A_{01} &= A_{10} = \frac{1}{2}(A_{\nu_e} - A_{\nu_\mu}) , \\ A_{44} &= A_{\nu_\tau} \end{aligned} \tag{B1}$$

and

$$\begin{aligned} A_{\bar{0}\bar{0}} &= A_{\bar{1}\bar{1}} = \frac{1}{2}(A_{\bar{\nu}_e} + A_{\bar{\nu}_\mu}), \\ A_{\bar{0}\bar{1}} &= A_{\bar{1}\bar{0}} = \frac{1}{2}(A_{\bar{\nu}_e} - A_{\bar{\nu}_\mu}) , \\ A_{\bar{4}\bar{4}} &= A_{\bar{\nu}_\tau} . \end{aligned} \tag{B2}$$

The nonzero B_a and $B_{\bar{a}}$ are

$$B_0 = \tilde{B}_{\nu_e} + \tilde{B}_{\nu_\mu}, \quad B_1 = \tilde{B}_{\nu_e} - \tilde{B}_{\nu_\mu}, \quad B_4 = \tilde{B}_{\nu_\tau} \tag{B3}$$

and

$$B_{\bar{0}} = \tilde{B}_{\bar{\nu}_e} + \tilde{B}_{\bar{\nu}_\mu}, \quad B_{\bar{1}} = \tilde{B}_{\bar{\nu}_e} - \tilde{B}_{\bar{\nu}_\mu}, \quad B_{\bar{4}} = \tilde{B}_{\bar{\nu}_\tau} . \tag{B4}$$

The remaining nonzero coefficients for neutrinos are

$$\begin{aligned} C_{00} &= \frac{1}{2}(\tilde{C}_{\nu_e\nu_e} + \tilde{C}_{\nu_\mu\nu_e} + \tilde{C}_{\nu_e\nu_\mu} + \tilde{C}_{\nu_\mu\nu_\mu}) , \\ C_{01} &= \frac{1}{2}(\tilde{C}_{\nu_e\nu_e} + \tilde{C}_{\nu_\mu\nu_e} - \tilde{C}_{\nu_e\nu_\mu} - \tilde{C}_{\nu_\mu\nu_\mu}) , \\ C_{10} &= \frac{1}{2}(\tilde{C}_{\nu_e\nu_e} - \tilde{C}_{\nu_\mu\nu_e} + \tilde{C}_{\nu_e\nu_\mu} - \tilde{C}_{\nu_\mu\nu_\mu}) , \\ C_{11} &= \frac{1}{2}(\tilde{C}_{\nu_e\nu_e} - \tilde{C}_{\nu_\mu\nu_e} - \tilde{C}_{\nu_e\nu_\mu} + \tilde{C}_{\nu_\mu\nu_\mu}) , \\ C_{04} &= (\tilde{C}_{\nu_e\nu_\tau} + \tilde{C}_{\nu_\mu\nu_\tau}), \quad C_{14} = (\tilde{C}_{\nu_e\nu_\tau} - \tilde{C}_{\nu_\mu\nu_\tau}) , \\ C_{40} &= \frac{1}{2}(\tilde{C}_{\nu_e\nu_\tau} + \tilde{C}_{\nu_\mu\nu_\tau}), \; C_{41} = \frac{1}{2}(\tilde{C}_{\nu_e\nu_\tau} - \tilde{C}_{\nu_\mu\nu_\tau}), \\ C_{44} &= \tilde{C}_{\nu_\tau\nu_\tau} , \\ C_{0\bar{0}} &= \frac{1}{2}(\tilde{C}_{\nu_e\bar{\nu}_e} + \tilde{C}_{\nu_\mu\bar{\nu}_e} + \tilde{C}_{\nu_e\bar{\nu}_\mu} + \tilde{C}_{\nu_\mu\bar{\nu}_\mu}) , \\ C_{0\bar{1}} &= \frac{1}{2}(\tilde{C}_{\nu_e\bar{\nu}_e} + \tilde{C}_{\nu_\mu\bar{\nu}_e} - \tilde{C}_{\nu_e\bar{\nu}_\mu} - \tilde{C}_{\nu_\mu\bar{\nu}_\mu}) , \\ C_{1\bar{0}} &= \frac{1}{2}(\tilde{C}_{\nu_e\bar{\nu}_e} - \tilde{C}_{\nu_\mu\bar{\nu}_e} + \tilde{C}_{\nu_e\bar{\nu}_\mu} - \tilde{C}_{\nu_\mu\bar{\nu}_\mu}) , \\ C_{1\bar{1}} &= \frac{1}{2}(\tilde{C}_{\nu_e\bar{\nu}_e} - \tilde{C}_{\nu_\mu\bar{\nu}_e} - \tilde{C}_{\nu_e\bar{\nu}_\mu} + \tilde{C}_{\nu_\mu\bar{\nu}_\mu}) , \\ C_{0\bar{4}} &= (\tilde{C}_{\nu_e\bar{\nu}_\tau} + \tilde{C}_{\nu_\mu\bar{\nu}_\tau}), \quad C_{1\bar{4}} = (\tilde{C}_{\nu_e\bar{\nu}_\tau} - \tilde{C}_{\nu_\mu\bar{\nu}_\tau}) , \\ C_{4\bar{0}} &= \frac{1}{2}(\tilde{C}_{\nu_e\bar{\nu}_\tau} + \tilde{C}_{\nu_\mu\bar{\nu}_\tau}), \quad C_{4\bar{1}} = \frac{1}{2}(\tilde{C}_{\nu_e\bar{\nu}_\tau} - \tilde{C}_{\nu_\mu\bar{\nu}_\tau}), \\ C_{4\bar{4}} &= \tilde{C}_{\nu_\tau\bar{\nu}_\tau} . \end{aligned} \tag{B5}$$

For antineutrinos, the remaining nonzero coefficients are

$$\begin{aligned} C_{\bar{0}\bar{0}} &= \frac{1}{2}(\tilde{C}_{\bar{\nu}_e\nu_e} + \tilde{C}_{\bar{\nu}_\mu\nu_e} + \tilde{C}_{\bar{\nu}_e\nu_\mu} + \tilde{C}_{\bar{\nu}_\mu\nu_\mu}) , \\ C_{\bar{0}\bar{1}} &= \frac{1}{2}(\tilde{C}_{\bar{\nu}_e\nu_e} + \tilde{C}_{\bar{\nu}_\mu\nu_e} - \tilde{C}_{\bar{\nu}_e\nu_\mu} - \tilde{C}_{\bar{\nu}_\mu\nu_\mu}) , \\ C_{\bar{1}\bar{0}} &= \frac{1}{2}(\tilde{C}_{\bar{\nu}_e\nu_e} - \tilde{C}_{\bar{\nu}_\mu\nu_e} + \tilde{C}_{\bar{\nu}_e\nu_\mu} - \tilde{C}_{\bar{\nu}_\mu\nu_\mu}) , \\ C_{\bar{1}\bar{1}} &= \frac{1}{2}(\tilde{C}_{\bar{\nu}_e\nu_e} - \tilde{C}_{\bar{\nu}_\mu\nu_e} - \tilde{C}_{\bar{\nu}_e\nu_\mu} + \tilde{C}_{\bar{\nu}_\mu\nu_\mu}) , \\ C_{\bar{0}4} &= (\tilde{C}_{\bar{\nu}_e\nu_\tau} + \tilde{C}_{\bar{\nu}_\mu\nu_\tau}), \quad C_{\bar{1}4} = (\tilde{C}_{\bar{\nu}_e\nu_\tau} - \tilde{C}_{\bar{\nu}_\mu\nu_\tau}) , \\ C_{\bar{4}0} &= \frac{1}{2}(\tilde{C}_{\bar{\nu}_e\nu_\tau} + \tilde{C}_{\bar{\nu}_\mu\nu_\tau}), \quad C_{\bar{4}1} = \frac{1}{2}(\tilde{C}_{\bar{\nu}_e\nu_\tau} - \tilde{C}_{\bar{\nu}_\mu\nu_\tau}), \\ C_{\bar{4}4} &= \tilde{C}_{\bar{\nu}_\tau\nu_\tau} , \\ C_{\bar{0}\bar{0}} &= \frac{1}{2}(\tilde{C}_{\bar{\nu}_e\bar{\nu}_e} + \tilde{C}_{\bar{\nu}_\mu\bar{\nu}_e} + \tilde{C}_{\bar{\nu}_e\bar{\nu}_\mu} + \tilde{C}_{\bar{\nu}_\mu\bar{\nu}_\mu}), \\ C_{\bar{0}\bar{1}} &= \frac{1}{2}(\tilde{C}_{\bar{\nu}_e\bar{\nu}_e} + \tilde{C}_{\bar{\nu}_\mu\bar{\nu}_e} - \tilde{C}_{\bar{\nu}_e\bar{\nu}_\mu} - \tilde{C}_{\bar{\nu}_\mu\bar{\nu}_\mu}) , \\ C_{\bar{1}\bar{0}} &= \frac{1}{2}(\tilde{C}_{\bar{\nu}_e\bar{\nu}_e} - \tilde{C}_{\bar{\nu}_\mu\bar{\nu}_e} + \tilde{C}_{\bar{\nu}_e\bar{\nu}_\mu} - \tilde{C}_{\bar{\nu}_\mu\bar{\nu}_\mu}) , \\ C_{\bar{1}\bar{1}} &= \frac{1}{2}(\tilde{C}_{\bar{\nu}_e\bar{\nu}_e} - \tilde{C}_{\bar{\nu}_\mu\bar{\nu}_e} - \tilde{C}_{\bar{\nu}_e\bar{\nu}_\mu} + \tilde{C}_{\bar{\nu}_\mu\bar{\nu}_\mu}) , \\ C_{\bar{0}\bar{4}} &= (\tilde{C}_{\bar{\nu}_e\bar{\nu}_\tau} + \tilde{C}_{\bar{\nu}_\mu\bar{\nu}_\tau}), \quad C_{\bar{1}\bar{4}} = (\tilde{C}_{\bar{\nu}_e\bar{\nu}_\tau} - \tilde{C}_{\bar{\nu}_\mu\bar{\nu}_\tau}) , \\ C_{\bar{4}\bar{0}} &= \frac{1}{2}(\tilde{C}_{\bar{\nu}_e\bar{\nu}_\tau} + \tilde{C}_{\bar{\nu}_\mu\bar{\nu}_\tau}), \quad C_{\bar{4}\bar{1}} = \frac{1}{2}(\tilde{C}_{\bar{\nu}_e\bar{\nu}_\tau} - \tilde{C}_{\bar{\nu}_\mu\bar{\nu}_\tau}) , \\ C_{\bar{4}\bar{4}} &= \tilde{C}_{\bar{\nu}_\tau\bar{\nu}_\tau} . \end{aligned} \tag{B6}$$

[1] See, for example, E. W. Kolb and M. S. Turner, *The Early Universe* (Addison-Wesley, Redwood City, CA, 1990).

[2] F. Boehm and P. Vogel, *The Physics of Massive Neutrinos*, 2nd ed. (Cambridge University Press, Cambridge, England, 1992).

[3] A. D. Dolgov, Yad. Fiz. **33**, 1309 (1981) [Sov. J. Nucl. Phys. **33**, 700 (1981)].

[4] L. Stodolsky, Phys. Rev. D **36**, 2273 (1987).

[5] P. Langacker, S. T. Petcov, G. Steigman, and S. Toshev, Nucl. Phys. **B282**, 589 (1987).

[6] D. Notzold and G. Raffelt, Nucl. Phys. **B307**, 924 (1988).

[7] M. J. Savage, R. A. Malaney, and G. M. Fuller, Astrophys. J. **368**, 1 (1991).

[8] K. Enqvist, K. Kainulainen, and J. Maalampi, Nucl. Phys. **B349**, 754 (1991).

[9] K. Enqvist, K. Kainulainen, and M. Thomson, Nucl. Phys. **B373**, 498 (1992).

[10] X. Shi, D. N. Schramm, and B. D. Fields, Phys. Rev. D **48**, 2563 (1993).
[11] V. A. Kostelecký, J. Pantaleone, and S. Samuel, Phys. Lett. B **315**, 46 (1993).
[12] V. A. Kostelecký and S. Samuel, Phys. Lett. B **318**, 127 (1993).
[13] V. A. Kostelecký and S. Samuel, Phys. Rev. D **49**, 1740 (1994).
[14] B. H. J. McKellar and M. J. Thomson, Phys. Rev. D **49**, 2710 (1994).
[15] S. Dodelson and M. S. Turner, Phys. Rev. D **46**, 3372 (1992); B. Fields, D. Dodelson, and M. S. Turner, *ibid.* **47**, 4309 (1993).
[16] A. D. Dolgov and M. Fukugita, Phys. Rev. D **46**, 5378 (1992).
[17] J. Pantaleone, Phys. Lett. B **287**, 128 (1992); Phys. Rev. D **46**, 510 (1992).
[18] G. Sigl and G. Raffelt, Nucl. Phys. **B406**, 423 (1993).
[19] S. Samuel, Phys. Rev. D **48**, 1462 (1993).
[20] L. Wolfenstein, Phys. Rev. D **17**, 2369 (1978); **20**, 2634 (1979); S. P. Mikheyev and A. Yu. Smirnov, Yad. Fiz. **42**, 1441 (1985) [Sov. J. Nucl. Phys. **42**, 913 (1985)]; Usp. Fiz. Nauk. **153**, 3 (1987) [Sov. Phys. Usp. **30**, 759 (1987)].
[21] V. A. Kostelecký and S. Samuel, Phys. Rev. D **52**, 621 (1995).